On the suitability of ~~general-purpose Finite-Volume~~ second-order accurate finite-volume solvers for the simulation of ~~Atmospheric-Boundary-Layer~~ atmospheric boundary layer flow

Beatrice Giacomini[1] and Marco G. Giometto[1]

[1]Department of Civil Engineering and Engineering Mechanics, Columbia University in the City of New York, 500 W 120th St, New York, NY 10027, USA.

Correspondence: Marco Giometto (mg3929@columbia.edu)

Abstract. ~~In the present work ,~~ The present work analyzes the quality and reliability of ~~a~~ an important class of general-purpose~~second-order-accurate Finite-Volume- (FV-) based solver are assessed in wall-modeled~~ , second-order accurate finite-volume (FV) solvers for the large-eddy ~~simulations~~ simulation of a neutrally-stratified ~~Atmospheric-Boundary-Layer~~ atmospheric boundary layer (ABL) flow~~with no Coriolis effects. The~~ . The analysis is carried out within the OpenFOAM® framework, which is based on a colocated grid arrangement. A series of open-channel flow simulations are performed using a static Smagorinsky model for sub-grid scale momentum fluxes and an algebraic equilibrium wall-layer model. The sensitivity of the solution to variations in numerical parameters such as grid resolution (up to 160^3 control volumes), numerical solvers, and interpolation schemes for the discretization of the nonlinear term is studied and ~~aspect ratio is analyzed, and~~ results are contrasted against those from a ~~well-proven mixed Pseudo-Spectral and Finite-Difference~~ well established mixed pseudo-spectral–finite-difference code. Considered flow statistics include the mean streamwise velocity, resolved Reynolds stress, turbulence intensities, skewness, kurtosis, spectra and spatial autocorrelations. ~~It is found that first-~~ The structure of mechanisms responsible for momentum transfer in the flow system is also discussed via a quadrant and a conditional-flow analysis. At the considered resolutions, the considered class of FV-based solvers yields a poorly correlated flow field and ~~second-order velocity statistics are sensitive to the grid resolution and to the details of~~ is not able to accurately capture the dominant mechanisms responsible for momentum transport in the ABL, especially when using linear interpolation schemes for the ~~near-wall numerical treatment, and a general improvement is observed with horizontal grid refinement. Higher-order statistics, spectra and autocorrelations of the streamwise velocity, on the contrary, are consistently mispredicted, regardless of the grid resolution. Skewness and kurtosis of the streamwise velocity, for instance, are overpredicted in the surface layer, whereas one-dimensional spectra feature a strong sensitivity to the grid resolution in the production range and a rapid decay of energy density at higher wavenumber. In addition, the typical signatures of Large-Scale Motions (LSMs) are absent in the premultiplied streamwise velocity spectra, the spatial autocorrelation functions rapidly decay along both the streamwise and spanwise coordinate directions, and instantaneous snapshots of the velocity field are populated by relatively short and thin streaks, confirming that the flow lacks LSMs. Further, the dominant mechanism supporting the tangential Reynolds stress in ABL flow – spanwise-paired~~ discretization of non-linear terms. The latter consist of sweeps and ~~ejections– is much weaker than what commonly observed in ABL flows, ejections are severely underpredicted, and sweeps account for most of the tangential Reynolds stress in the surface layer, which is at~~

odds with available measurements and with corresponing results from the PSFD-based solver. The inability of the solver to correctly capture the spatially-localized and relatively strong ejection events, in the authors' opinion, is the root-canse of many of the observed mismatches and sensitivity of flow statistics to grid resolution. The present findings show that truncation errors have an overwhelming impact on the predictive capabilities of second-order-accurate FV-based solvers, introducing a degree of uncertainty in model results that may be difficult to quantify across applications involving boundary-layer flows. Although mean flow and second-order statistics become acceptable provided sufficient ejection pairs organized side by side along the cross-stream direction, representative of a streamwise roll mode. This shortcoming leads to a misprediction of flow statistics that are relevant for ABL applications and to an enhanced sensitivity of the solution to variations in grid resolution, the use of said solvers might prove problematic for studies requiring accurate higher-order statistics, velocity spectra and turbulence topologycalling for future research aimed at reducing the impact of modeling and discretization errors.

1 Introduction

An accurate prediction of Atmospheric Boundary Layer atmospheric boundary layer (ABL) flows is of paramount importance across a wide range of fields and applications, including weather forecasting, complex-terrain complex terrain meteorology, agriculture, air quality modeling and wind energy (Fernando, 2010; Whiteman, 2000; Oke et al., 2017; Calaf et al., 2010a; Shaw et al., 201 . There is indeed a rapidly growing interest in these applications, motivated by the increasing need for high-resolution information on turbulence and turbulent transport across scales, for the prediction of severe-weather events (hurricanes, heat waves) and for the design of mitigation strategies against climate change. (Whiteman, 2000; Fernando, 2010; Calaf et al., 2010a; Oke et al., 2017; Shaw et .

Since the early work of Deardorff (1970), the Large-Eddy-Simulation large eddy simulation (LES) technique has spurred considerable insight on the fundamental dynamics of ABL flows. In LESs, only the motions at large scales are directly resolved on the given grid, often dictated by the available computational resources, whereas contributions from Sub-Grid-Scale (SGS) motions to momentum and mass transport and energy dissipation are parameterized as functions of resolved-scale quantities. In the last few decades, the increased availability and power of high-performance-computing facilities (national supercomputers, cloud-based services, etc.) have led to a proliferation of LES studies of ABL processes. These studies include fundamental analysis of the ABL flow over rough surfaces (Bou-Zeid et al., 2009; Anderson and Meneveau, 2010; Salesky et al., 2017; Momen et al., 2 (Anderson and Meneveau, 2010; Salesky et al., 2017; Momen et al., 2018), over and within plant canopies (Yue et al., 2007b; Chester et al and urban canopies (Tseng et al., 2006; Bou-Zeid et al., 2009; Cheng and Porté-Agel, 2013; Li et al., 2016b; Giometto et al., 2017; Nazari , and the investigation of the (Yue et al., 2007b; Bailey and Stoll, 2013; Pan et al., 2014; Tseng et al., 2006; Bou-Zeid et al., 2009; Giomett , and ABL flow for wind energy applications (Calaf et al., 2010b; Sharma et al., 2016; Abkar and Porté-Agel, 2013; Stevens and Meneveau (Calaf et al., 2010a; Abkar and Porté-Agel, 2013; Stevens and Meneveau, 2017), amongst others.

When it comes to the simulation of ABL flows, fully- or partially-dealiased mixed Pseudo-Spectral- and Finite-Difference-(PSFD-) based solvers have been the

The majority of past works has relied on fully or partially dealiased mixed pseudo-spectral–finite-difference (PSFD) solvers—the go-to approach since the studies for LES studies since the works of Moin et al. (1978) and Moeng (1984). Such solvers combine the accuracy and efficiency of the Fourier partial-sum representation in the horizontal coordinate directions with the more flexible Finite-Difference approach in the vertical (non-periodic) one. Nowadays, most LESs of ABL flows still rely on PSFD-based solvers (see e.g., Sullivan et al., 1994; Albertson and Parlange, 1999). These solvers Such solvers are known to yield accurate flow fields up to the LES cut-off cutoff frequency and to produce good results when used in conjunction with dynamic SGS sub-grid scale (SGS) models (Germano et al., 1991; Lilly, 1992), even when relying on a low-order Finite-Difference finite-difference discretization in the vertical coordinate direction. However, single-domain single domain PSFD-based solvers are limited to regular domainsand, in general, , are not suitable for accurately representing the simulation of non-periodic flows and sharp variations in the flow field , such as shocks or gas-solid interfaces. In addition, problematics may arise when parallel computing is attempted (Canuto et al., 2006; Margairaz et al., 2018), and typically feature poor scaling owing to the global support of their spatial representation (see e.g. Margairaz et al., 2018). With the increasing need to account for complex geometries and multi-physics, several efforts have been devoted to the mitigation of the aforementioned limitations . For example, Fang et al. (2011) and Li et al. (2016a) devised strategies to alleviate the Gibbs oscillations that arise when using Pseudo-Spectral expansions in multiply-connected domains, whereas in Chester et al. (2007a) a fringe-forcing technique was proposed to simulate non-periodic flows within a Fourier-based Pseudo-Spectral solver. A shortcoming of these formulations is that they (Fang et al., 2011; Li et al., 2016a; Chester et al., 2007a). The solutions, however, are often ad-hoc or validated only for specific applications, thus introducing a degree of uncertainty in model results and conservation properties of the numerical scheme that might be that is hard to quantify and generalize.

There is hence a growing interest in using computational-fluid-dynamics solvers for LES from the ABL community in LES solvers based on compact spatial schemes via structured or unstructured meshes (Orlandi, 2000; Ferziger and Peric, 2002). The Parallelized Large-Eddy Simulation model (Raasch and Schröter, 2001; Maronga et al., 2015) and the Weather Research and Forecasting model (Skamarock et al., 2008; Chen et al., 2011) parallelized large eddy simulation model (Raasch and Schröter, 2001; Maro and the weather research and forecasting model (Skamarock et al., 2008; Powers et al., 2017) are prominent examples of said efforts. Both the approaches are based on a high-order Finite-Difference discretization , whereby a system of dynamical solvers is combined to simulate a range of meteorological phenomena. The resulting solvers are relatively versatile, suitable for complex geometries via structured and unstructured meshes, able to support local grid refinement and relatively straightforward to parallelize, given the compact nature of the spatial discretization. Nonlinear terms are typically finite-difference discretization and nonlinear terms are approximated by using high-order upwind-biased differencing schemes, which upwind biased differencing schemes. The latter are suitable for LES in complex geometries with arbitrary grid stretching factors and outflow boundary conditions (Beaudan and Moin, 1994; Mittal and Moin, 1997). Such schemes, however, are known to be overly , but are dissipative and do not strictly conserve energy. In addition, while satisfactory first- and second-order flow statistics can be obtained in complex geometries at moderate Reynolds numbers (Mittal and Moin, 1997), the excessive damping of resolved-scale energy

at high wavenumber is likely to compromise their predictive capabilities for high-Reynolds ABL-flow applications. On the other hand, if central schemes are used instead for the evaluation of nonlinear terms, no numerical dissipation is introduced, but truncation errors can have an overwhelming impact on the computed flow field (Ghosal, 1996; Kravchenko and Moin, 1997), especially in simulations where the grid is just fine enough to resolve the large-scale flow structures. . These limitations typically result in a strong sensitivity of the solution to properties of the spatial discretization and of the numerical scheme (Vuorinen et al., 2014; Rezaeiravesh and Liefvendahl, 2018; Breuer, 1998; Montecchia et al., 2019)numerical scheme (Meyers et al., 2006; Meyers and B.J. Geurts, 2007; Meyers and Sagaut, 2007; Vuorinen et al., 2014; Rezaeiravesh and Liefvendahl, 2018 . Further, truncation errors corrupt the high-wavenumber high wavenumber range of the solution, also complicating the use of restricting the ability to adopt dynamic LES closure models whereby the which make use of information from the small smallest resolved scales of motion is leveraged to evaluate the SGS diffusion (Germano et al., 1991). Notwithstanding these limitations, such central schemes have been heavily employed in the past in both the geophysical and engineering flow communities, and are the de-facto standard in the wind engineering one, where most of the numerical simulations are carried out using second-order-accurate Finite-Volume- (FV-) based solvers (Nilsson et al., 2008; Stovall et al., 2010; Churchfield et al., 2010; Balogh et al., . Note that the studies conducted with FV-based solvers are mainly focused on first- and second-order flow statistics, which are themselves not sufficient to fully characterize turbulence – and related transport – in the ABL. accurate finite-volume (FV) -based solvers (Stovall et al., 2010; Churchfield et al., 2010; Balogh et al., 2012; Churchfield et al., 2013; Shi and Yeo, 2016, 2017; García .

The Motivated by the aforementioned needs, the present study aims at bridging this knowledge gap by analyzing characterizing the quality and reliability of a second-order-accurate FV solver an important class of second-order accurate FV solvers for the LES of ABL flow, with a lens on higher-order statistics, energy spectra, spatial autocorrelations and turbulence topologyneutrally-stratified ABL flows. The analysis is carried out leveraging the conducted in the open-channel flow setup (no Coriolis acceleration) via the OpenFOAM® framework (Weller et al., 1998; De Villiers, 2006; Jasak et al., 2007). A suite of simulations is carried out whereby varying physical and numerical parametersare varied. The predictions from the solver , including grid resolution (up to 160^3 control volumes), the solver, and interpolation schemes for the discretization of the non-linear terms. Predictions from the FV solvers are contrasted against the results from the Albertson and Parlange (1999) PSFD code . in terms of first-, second-, and higher-order statistics, energy spectra, spatial autocorrelations, and mechanisms supporting momentum transport. The end goal is to provide a more nuanced understanding of the capabilities of general-purpose, second order, FV-based solvers in predicting ABL flow.

The work is organized as follows. Section 2 briefly summarizes the governing equations, the numerical methods and the set-up setup of the problem, along with a description summary of the simulated cases and of the post-processing procedure. The results are proposed Results are shown in §3 . The and conclusions are drawn in §??. In the Appendix, the 4. A discussion on the sensitivity of the solution to model constants, interpolation schemes and numerical solvers is reportedprovided in the Appendix.

2 Methodology

2.1 Governing equations and numerical schemes

In the following, vector and index notations are used interchangeably, according to needs, in a Cartesian reference system. The spatially-filtered ~~Navier-Stokes~~ Navier–Stokes equations are considered,

$$\nabla \cdot \mathbf{u} = 0 \,, \tag{1}$$

$$\frac{\partial \mathbf{u}}{\partial t} + \nabla \mathbf{u} \cdot \mathbf{u} = -\frac{1}{\rho}\nabla \tilde{p} + \nabla \cdot \boldsymbol{\tau} - \nabla \cdot \boldsymbol{\tau}^{SGS,dev} - \frac{1}{\rho}\nabla P \,, \tag{2}$$

where ~~$\mathbf{u} = (u_1, u_2, u_3)$~~ $\mathbf{u} = (u_x, u_y, u_z) = (u, v, w)$ is the spatially-filtered velocity field along the streamwise ~~(x_1)~~ (x), cross-stream (y) and vertical ~~(x_2) and spanwise (x_3)~~ (z) coordinate directions, t is the time, ρ is the ~~(constant) fluid density~~ constant fluid density (Boussinesq approximation), $\tilde{p} \equiv p + \frac{1}{3}\tau_{kk}^{SGS}$ is the pressure term with an additional contribution from the ~~Sub-Grid~~ sub-grid kinetic energy ($\frac{1}{2}\tau_{kk}^{SGS}$), $\boldsymbol{\tau}$ is the filtered ~~viscous-stress~~ viscous stress tensor, $\boldsymbol{\tau}^{SGS,dev}$ is the deviatoric part of the ~~SGS-stress~~ SGS stress tensor. In addition, the term $-\frac{1}{\rho}\nabla P$ is a ~~constant~~ pressure gradient, here assumed to be constant and uniform, responsible for driving the flow. The filtered viscous tensor is $\boldsymbol{\tau} = -2\nu\mathbf{S}$, where $\nu = \text{const}$ is the kinematic viscosity of the Newtonian fluid and $\mathbf{S}$ is the resolved (in the LES sense) ~~rate-of-strain~~ rate of strain tensor. For the ~~SGS-stress~~ SGS stress tensor, the static Smagorinsky model is used,

$$\boldsymbol{\tau}^{SGS,dev} = -2\nu^{SGS}\mathbf{S} = -2(C_S\Delta)^2|\mathbf{S}|\mathbf{S} \,, \tag{3}$$

where ν^{SGS} is the SGS eddy viscosity, C_S is the Smagorinsky coefficient (Smagorinsky, 1963), ~~$\Delta = (\Delta x_1 \Delta x_2 \Delta x_3)^{1/3}$~~ $\Delta = (\Delta x \Delta y \Delta z)^{1/3}$ is a local ~~length-scale~~ length scale based on the volume of the computational cell (Scotti et al., 1993), and $|\mathbf{S}| = \sqrt{2\mathbf{S} : \mathbf{S}}$ quantifies the magnitude of the rate of strain. In the present work, $C_S = 0.1$, unless otherwise specified. ~~The authors would like to point out~~ Note that dynamic Smagorinsky models are ~~in general~~ preferred to the static one for the LES of ABL flows (Germano et al., 1991; Lilly, 1992; Meneveau et al., 1996; Porté-Agel, 2004; Bou-Zeid et al., 2005). Dynamic models evaluate SGS stresses via first-principles-based constraints, feature improved dissipation properties when compared to the static Smagorinsky one (especially in the vicinity of solid boundaries)~~and, foremost, are parameter-free~~, and are free of explicit modeling parameters. The choice made in the present study is motivated by problematics encountered when using the available dynamic Lagrangian model in preliminary tests. ~~Note that, however,~~ However, while SGS dissipation plays a crucial role in PSFD solvers, truncation errors ~~typically~~ may overshadow SGS stress contributions in the second-order FV-based ones (Kravchenko and Moin, 1997). The static Smagorinsky SGS model used herein might hence perform similarly to dynamic SGS models for the considered flow ~~set-up. This observation~~ setup. This conjecture is supported by the results of Majander and Siikonen (2002).

The ~~large-scale~~ large scale separation between near-surface and outer-layer ~~energy-containing~~ energy containing ABL motions poses stringent resolution requirements to numerical modelers~~if all of the energy-containing motions necessitate~~, if all the

energy containing motions have to be resolved. To reduce the computational cost of such simulations, the near-surface region is typically bypassed, and a phenomenological wall-layer model is leveraged instead to account for the impact of near-wall (inner-layer) dynamics on the outer-layer flow ~~(Mason, 1994; Piomelli and Balaras, 2002; Piomelli, 2008; Bose and Park, 2018)~~(Piomelli, 2008; I . This approach is referred to as ~~Wall-Modeled Large-Eddy Simulation~~ wall-modeled large eddy simulation (WMLES) ~~,~~ and is used herein. ~~ABL flows are typically in fully-rough aerodynamic regime with the underlying surface (Stull, 1988), hence a rough-wall wall-layer model is required to close the equations at the surface. Such a procedure is standard practice in WMLES of ABL flows (see e.g., Albertson and Parlange, 1999). In the present work, an~~ An algebraic wall-layer ~~equilibrium~~ model for surfaces in ~~fully-rough aerodynamic regime has been~~ fully rough aerodynamic regime was implemented, based on the logarithmic ~~law of the wall,~~ equilibrium assumption, i.e.,

$$|\mathbf{u}| = \frac{u_\tau}{\kappa}\frac{u_*}{\kappa}\ln\left(\frac{x_2}{x_{2,0}}\frac{z}{z_0}\right), \tag{4}$$

where ~~$|\mathbf{u}| = \sqrt{u_1^2 + u_3^2}$~~ $|\mathbf{u}| \equiv \sqrt{u^2+v^2}$ is the norm of the velocity at a certain distance from the ground level, ~~u_τ~~ u_* is the friction velocity (see Sub-Section 2.2 for details), κ is the von Kármán constant, ~~x_2~~ z is the distance from the ground level and ~~$x_{2,0}$~~ z_0 is the so-called aerodynamic roughness length, ~~which quantifies~~ a length-scale used to quantify the drag of the underlying surface. ~~Here,~~ In this work we define $\kappa = 0.41$ and ~~$x_{2,0} = 0.1$ m. Specifically, the~~ $z_0 = 0.1$ m. The kinematic wall shear stress is assumed to be proportional to the local velocity gradient (Boussinesq ~~approximation~~hypothesis),

$$\tau_{\alpha 2, w i z, w} = (\nu + \nu_t)\frac{\partial u_\alpha}{\partial x_2}\frac{\partial u_i}{\partial z}\Big|_w = (\nu+\nu_t)\frac{u_\alpha}{x_2}, \quad \alpha i = 1x, 3y\,, \tag{5}$$

with ν_t being the total eddy viscosity. Employing the no-slip condition for the velocity field, the standard FV approximation of the shear stress at the wall gives (Mukha et al., 2019)

$$\tau_{iz,w} = (\nu+\nu_t)_f\frac{u_{i,c}}{\Delta z}, \quad i = x, y\,, \tag{6}$$

where the subscript f is used to denote the evaluation at the center of the wall face, the subscript c denotes the evaluation at the center of the wall-adjacent cell and Δz is the distance from the wall. From the ~~log-law~~ logarithmic law (Eq. 4) evaluated at the first cell-center, one can write ~~$u_\tau = (\kappa|\mathbf{u}|)/(\ln(x_2/x_{2,0})$~~ $u_* = \kappa|\mathbf{u}|_c/\ln(\frac{\Delta z}{z_0})$. Using the definition of friction velocity ~~$u_\tau = \sqrt{\tau_{\alpha 2,w}|\mathbf{u}|/u_\alpha}$ for $\alpha = 1, 3$ (no summation over repeated indices)~~ $u_* = \sqrt{\tau_w^2}$, where τ_w is the magnitude of the kinematic wall shear stress vector, along with Eq. 5 and rearranging terms, the total eddy viscosity ~~reads~~ at the wall can be written as

$$\nu_{tt,f} = \left(\frac{\kappa|\mathbf{u}|}{\ln\left(\frac{x_2}{x_{2,0}}\right)}\frac{\kappa|\mathbf{u}|_c}{\ln\left(\frac{\Delta z}{z_0}\right)}\right)^2\frac{x_2}{|\mathbf{u}|}\frac{\Delta z}{|\mathbf{u}|_c} - \nu\,, \tag{7}$$

which is the formulation implemented herein. Note that $\nu + \nu_t \approx \nu_t$ in ~~boundary-layer flows in fully-rough~~ boundary layer flows in fully rough aerodynamic regime, so that ν could be neglected without loss of accuracy.

In the OpenFOAM® framework, ~~considered in the present work, the FV method is used on a co-located grid. The integral version of~~ the ~~filtered Navier-Stokes equations is solved on every control volume , leveraging~~ computational grid is colocated. Although advantageous in complex domains when compared to staggered grids (Ferziger and Peric, 2002), the colocated arrangement is known to cause difficulties with pressure-velocity coupling, hence requiring specific procedures to avoid oscillations in the solution. The standard Rhie-Chow correction (Rhie and Chow, 1983) is here adopted, which is known to negatively affeect the energy-conservation properties of central schemes (Ferziger and Peric, 2002). In addition, when approximating the integrals over the surfaces bounding each control volume (as a consequence of the Gauss divergence theorem~~to relate volume integrals to surface integrals. Unknowns~~), the unknowns are evaluated at face-centers and are assumed to be constant ~~on~~ at each face, yielding an overall second-order spatial accuracy (Churchfield et al., 2010). ~~A range of interpolation schemes is available, spanning from first-order upwind to higher-order ones. The linear interpolation scheme is considered herein, unless otherwise stated. Simulations are carried out using the PISO fractional step method to solve the system of equations (Issa, 1985) ,~~ Since the divergence form of the convective term is used in combination with a low-order scheme over a non-staggered grid, the solution is inherently unstable (Kravchenko and Moin, 1997). The present work makes use of the linear and the QUICK interpolation schemes (Ferziger and Peric, 2002) to evaluate the unknowns at face-centers (more details are provided in § 2.2). The numerical solver combines the PISO algorithm (Issa, 1985) for the pressure-velocity calculation and an implicit ~~Adams-Moulton time-stepping scheme is chosen~~ Adams–Moulton scheme for time integration (Ferziger and Peric, 2002). The performances of an alternative solver characterized by a Runge–Kutta time-advancement scheme and a projection method for the pressure-velocity coupling (Vuorinen et al., 2014) are also analyzed in the Appendix A2.

2.2 Problem ~~set-up~~setup

~~An extensive series of WMLESs~~ A series of WMLES of ABL flow (~~open-channel-flow set-up~~open-channel flow setup) is performed. Tests are carried out in the domain $[0, L_1] \times [0, L_2] \times [0, L_3]$ ~~with $L_1 = 2\pi h$, $L_2 = h$, $L_3 = \frac{4}{3}\pi h$~~ $[0, L_x] \times [0, L_y] \times [0, L_z]$ with $L_x = 2\pi h$, $L_y = \frac{4}{3}\pi h$, $L_z = h$, where $h = 1000$ m denotes the width of the open channel. ~~The symmetric boundary condition is imposed on~~ Symmetry is imposed at the top of the computational domain, no-slip applies at the lower surface ~~,~~ and periodic boundary conditions are enforced along each side. A kinematic pressure gradient term $-\frac{1}{\rho}\partial P/\partial x_1 = 1\ \mathrm{m/s^2}$ $-\frac{1}{\rho}\partial P/\partial x = 1\ \mathrm{m/s^2}$ drives the flow along the ~~x_1~~ x coordinate direction, yielding ~~$u_\tau = 1$ m/s~~ $u_* = 1$ m/s. The kinematic viscosity is set to ~~10^{-7} m^2/s in the bulk of the flow, resulting in $Re_\tau = 10^7$~~ a nominal value of 10^{-7} m^2/s, which results in an essentially inviscid flow.

~~Five cases are run, spanning different grid resolutions and aspect ratios. The~~ The computational mesh is Cartesian, with a uniform stencil along each direction. ~~In the following, N_i denotes the number of cell-centers along the i-th direction. The baseline calculation B-2π is performed~~ Three simulations are run, over 64^3 ~~control volumes. Two cases with the same aspect ratio $\Delta x_1/\Delta x_2 = 2\pi$ are run– the simulation C-2π over a coarser grid (32^3 control volumes) and the simulation F-2π over a finer grid (~~, 128^3 ~~control volumes). Two additional cases are considered~~ and 160^3 control volumes, with the ~~same number of grid~~

Table 1. Tabulated list of cases.

~~label~~ simulation	~~C-2π~~ FV64	~~B-4π~~ FV128	~~B-2π~~ FV160	~~B-π~~ FV64*	~~F-2π~~ FV128*
grid resolution	~~$32 \times 32 \times 32$~~ 64^3	~~$32 \times 64 \times 32$~~ 128^3	~~$64 \times 64 \times 64$~~ 160^3	~~$128 \times 64 \times 128$~~ 64^3	~~$128 \times 128 \times 128$~~ 128^3
numerical solver	~~π~~ FV	~~2π~~ FV	~~2π symbol~~ FV	~~dashed line~~ FV + QUICK	~~dash-dotted line~~ FV + QUICK

~~points along the vertical direction as in B-2π and different aspect ratios– the simulation B-4π, with aspect ratio $\Delta x_1/\Delta x_2 = 4\pi$ ($N_1 \times N_2 \times N_3 = 32 \times 64 \times 32$), and the simulation B-$\pi$, with aspect ratio $\Delta x_1/\Delta x_2 = \pi$ ($N_1 \times N_2 \times N_3 = 128 \times 64 \times 128$).~~ linear interpolation scheme for the evaluation of the unknowns at the face-centers (simulations FV64, FV128 and FV160, respectively). Three additional simulations are run, over the same grid resolutions, with the linear scheme for the approximation of every term except for the nonlinear one, for which the QUICK scheme is used instead (simulations FV64*, FV128* and FV160*). The cases span different grid resolutions at the same aspect ratio $\Delta x/\Delta z = 2\pi$. Note that the ~~grid-aspect-ratio sensitivity analysis is carried out by refining the grid only along the horizontal directions, in line with the approach of Park and Moin (2016). Preliminary tests indeed showed that, for the given resolution, ABL flow statistics are more sensitive to variations in the horizontal grid stencil and aspect ratio than in the vertical ones. The~~ chosen grid resolutions are in line with those typically used in studies of ABL flows using a pseudo-spectral approach (see, e.g., Salesky et al., 2017). All the calculations satisfy the ~~Courant-Friedrichs-Lewy~~ Courant–Friedrichs–Lewy (CFL) condition $Co \lesssim 0.1$, where Co is the Courant number. Runs are initialized from a ~~fully-developed open-channel-flow simulation at equilibrium~~fully developed open-channel flow simulation in statistically steady state (dynamic equilibrium), and time integration is carried out for 100 eddy turnover times, where the eddy turnover time is defined as h/u_τ. Flow statistics are the result of an averaging procedure in the horizontal plane of statistical homogeneity of turbulence (~~x_1x_3~~xy) and in time over the last 60 eddy turnover times. The procedure yields well converged statistics throughout the considered cases. In the following, the ~~space/time~~ horizontal and temporal averaging operation is denoted by $\langle\cdot\rangle$.

Results ~~in~~ from the present study are contrasted against corresponding ones from the Albertson and Parlange (1999) mixed PSFD code ~~. Said~~ (simulations PSFD64, PSFD128 and PSFD160). The code is based on an explicit ~~second-order-accurate Adams-Bashforth~~ second-order accurate Adams–Bashforth scheme for time integration and on a fractional-step method for solving the system of equations. ~~A single run, the reference simulation R-2π, was carried out with the PSFD solver at a resolution of 64^3 co-location nodes,~~ Simulations from the PSFD solver are carried out using a static Smagorinsky SGS model with $C_s = 0.1$, a rough wall-layer model with ~~$x_{2,0} = 0.1$ m, $z_0 = 0.1$ m, and~~ $Co \lesssim 0.1$~~, and the same initialization and averaging procedure as the one considered for the FV runs~~. A summary of the ~~simulated cases~~ runs is given in Tab. 1 along with the acronyms used in this study.

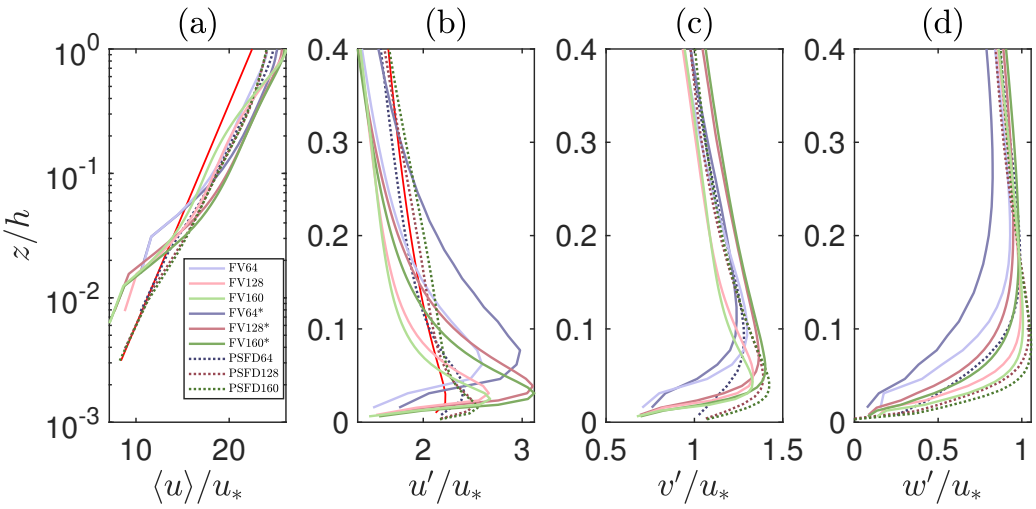

Figure 1. Vertical structure of mean streamwise velocity $\langle u \rangle / u_*$ (a), streamwise velocity RMS (b), cross-stream velocity RMS (c) and vertical velocity RMS (d). The red line in (a) denotes the reference logarithmic profile and the red line in (b) is a reference profile from Hultmark et al. (2013).

3 Results

This Section is devoted to the analysis of velocity ~~statistics~~central moments (§3.1), spectra and ~~autocorrelations from the second-order FV-based solver, along with detailed considerations on turbulence topology~~ spatial autocorrelations (§3.2), and momentum transfer mechanisms ~~. Mean streamwise velocity, resolved Reynolds stresses and higher-order statistics are discussed in §??. Sub-Section ?? focuses on velocity spectra and spatial autocorrelations, and a discussion on the turbulence topology based on conditionally-averaged flow field and quadrant analysis can be found in §??.~~ (§3.3).

3.1 Mean velocity, Reynolds stresses, and higher order statistics

3.2 ~~Mean profiles~~

~~In Fig. ??, the vertical structure of the normalized~~ The mean streamwise velocity ~~($\langle u_1 \rangle^+$) and resolved shear Reynolds stress ($-\langle u_1' u_2' \rangle^+$) is shown for all of the considered cases. The mean streamwise~~ is shown in Fig. 1(a), in a comparison with the phenomenological logarithmic-layer profile. The velocity at the first two cell-centers off the wall is consistently underpredicted, whereas a positive ~~Log-Layer Mismatch~~ log-layer mismatch (LLM) is observed in the bulk of the flow (Kawai and Larsson, 2012). The LLM is particularly pronounced for the cases using the QUICK interpolation scheme. This behavior could have been anticipated, as the wall shear stress is evaluated using the instantaneous horizontal velocity at the first cell-center off the wall. A number of procedures ~~has~~ have been proposed to alleviate the LLM, including modifying the ~~SGS-stress~~ SGS stress model in the near-wall region (Sullivan et al., 1994; Porté-Agel et al., 2000; Chow et al., 2005; Wu and Meyers,

2013), shifting the matching location further away from the wall (Kawai and Larsson, 2012), and carrying out a local horizontal/temporal filtering operation (Bou-Zeid et al., 2005; Xiang et al., 2017). In preliminary runs, we implemented the approach of Kawai and Larsson (2012) in an attempt to alleviate the authors applied the same approach as in Kawai and Larsson (2012) to mitigate the LLM, but observed an enhanced sensitivity of mean velocity profiles no apparent improvement was observed and the solution became very sensitivity to grid resolution and matching locationthat suggested that . This finding suggests that alternative procedures might work better for the considered solver. The results herein proposed are hence representative of the OpenFOAM® solver with the standard wall-layer treatment— need to be devised to overcome the LLM in ABL flow simulations using the considered class of FV solvers. Note that profiles from the set-up that is most commonly adopted when using this code (see, for instance, Churchfield et al. (2010); Shi and Yeo (2017)). Note that a positive LLM is observed even when using the PSFD solver also feature a positive LLM, in spite of a spatial, low-pass filtering operation that is carried out on the horizontal velocity before the evaluation of the field before evaluating the surface shear stress (Bou-Zeid et al., 2005). The one

The vertical structure of turbulence intensities is also shown in Fig.**??**(a) is indeed the expected mean velocity profile for PSFD solvers coupled with the static Smagorinsky model (see Meneveau et al., 1996; Bou-Zeid et al., 2005) and advocates for the use of alternative strategies to overcome the LLM therein as well. In Fig. **??**(b) , resolved Reynolds stresses are compared to the theoretical profile of the total stress $\tau_{12}^{tot} = (-\langle u_1' u_2' \rangle + \tau_{12}^{SGS} + \tau_{12}) = u_\tau^2 (1 - x_2/h)$. The profiles 1, where $(\cdot)'$ denotes the root mean square (RMS) of the fluctuations. Profiles from the FV-based solver feature a strong sensitivity to grid resolution and aspect ratio, and start off relatively slow from at the wall when compared to those from the PSFD one, throughout all the considered cases. For instance, at $x_2/h \approx 0.01$, the resolved Reynolds stresses from the R-2π case account for 21% of the total shear stress, whereas they account for only 2% in the corresponding B-2π case, 6% in the B-π case, and 8% in the F-2π one. PSFD-based solver and to the reference profile from Hultmark et al. (2013). This behavior is likely due to truncation errorsthat due to a combination of SGS and discretization errors, which damp the energy of high-wavenumber momentum-carrying modes in the near-surface region (see discussion in §**??**), which controls in large part the overall solution (Van Driest, 1956; Kawai and Larsson, 2012). The present results suggest that the impact of the SGS model on the global solution might be larger for FV-based solvers than for PSFD-based ones via SGS near-wall effects. This conclusion, however, is at odds with some of the numerical experiments that were conducted, where the solution was found to be poorly sensitive– when compared to the one from the PSFD-based solver– to details of the near-wall numerical procedure (e.g., using or not a wall-damping function) . Truncation errors might again be responsible for said behavior.

Vertical structure of mean streamwise velocity $\langle u_1 \rangle^+ = \langle u_1 \rangle / u_\tau$ (a) and resolved stress $\langle u_1' u_2' \rangle^+ = \langle u_1' u_2' \rangle / u_\tau^2$ (b). Red lines denote the phenomenological logarithmic-layer profile (a) and the theoretical profile for the total Reynolds stress (b). The other lines and symbols are defined in Table 1.

Turbulence intensities are shown in Fig. **??**, where $(\cdot)'$ denotes the Root Mean Square (RMS) of the fluctuations and $(\cdot)'^+ \equiv (\cdot)'/u_\tau$. The profiles are extremely sensitive to the grid resolution in the horizontal coordinate directions and start off relatively slow at the wall modes and whose accurate quantification remains an open challenge in LES (see e.g., Meyers et al., 2006; Meyers . Further aloft, u' (w') features relatively stronger (weaker) peak values when compared to the R-2π case and to the reference

Table 2. Relative error on the turbulence intensities $||u' - u'_{\text{ref}}||_{L^2}/||u'_{\text{ref}}||_{L^2}$ w.r.t. the reference profile from Hultmark et al. (2013), in the interval $z_0/h \leq z/h \leq 0.4$.

simulation	FV64	FV128	FV160	FV64*	FV128*	FV160*	PSFD~~solver, both in terms of shape and magnitude. 64~~	~~F~~
relative error on u'	0.2259	0.1696	0.1722	0.2808	0.2036	0.1965	0.1050	

~~profilefrom Hultmark et al. (2013). As a result, the velocity fluctuations are consistently underpredicted in the very near-wall region ($x_2/h \leq 0.025$). On the contrary, the $u_1'^+$-peak values are overpredicted, whereas the $u_2'^+$- and $u_3'^+$- peak values are underpredicted, except for the finest horizontal-grid-resolution runs (cases B-π and F-2π)~~corresponding PSFD profile, the overprediction (underprediction) being more apparent in the simulations with the QUICK scheme. The overshoot in the peak of ~~$u_1'^+$ and the underestimation of $u_2'^+$ and $u_3'^+$ in the surface-layer region are~~ u' is a well-known problem of FV-based WM-LES (Bae et al., 2018). Lack of energy redistribution via pressure fluctuation from ~~shear-generated $u_1'^+$ to $u_2'^+$ and $u_3'^+$~~ shear generated u' to v' and w' is the root cause of said behavior, and possible mitigation strategies include allowing for wall transpiration ~~(Bose and Moin, 2014; Bae et al., 2018)~~(Bose and Moin, 2014). Grid refinement ~~in the horizontal directions leads to an improved matching between the FV and~~ shifts the velocity RMS peaks closer to the surface and increases the magnitude of velocity RMS therein, but lead to no improvement in the $\max(u')$ and only marginally improves the estimation of the $\max(w')$. A quantitative measure of the relative error on u' with respect to the reference profile from Hultmark et al. (2013) in the $z_0/h \leq z/h \leq 0.4$ interval is shown in Tab. 2. It is clear that the PSFD solver performs best and that the FV solution with QUICK performs worst, but what's more important is that the convergence is not monotonic. Non monotonic convergence is relatively common in LES at relatively coarse resolutions and is due to the interaction between discretization and modeling errors, whose impact on the solution cannot be a-priori quantified (Meyers and B.J. Geurts, 2007).

~~Vertical structure of streamwise velocity RMS (a), vertical velocity RMS (b) and spanwise velocity RMS (c). Lines and symbols are defined in Table 1. The red line denotes the reference profile from Hultmark et al. (2013).~~

Skewness and kurtosis of the streamwise velocity (~~S_1 and K_1~~ S_{uu} and K_{uu}, respectively) are shown in Fig. **??**~~, along with the transfer efficiency coefficient, $r_{12} = -\langle u_1' u_2' \rangle / (u_1' u_2')$. Average values of said flow statistics in the surface layer are shown in Tab. **??**, where spurious near-wall effects are neglected by constraining the averaging to the interval $0.2 \leq x_2/h \leq 0.4$. Recall that the constancy of $S_1 \approx -0.3$, $K_1 \approx 3$, and $r_{12} \approx 0.3$ in the surface layer of the ABL is a manifestation of the self-similar nature of ABL turbulence therein (Del Álamo et al., 2006). 2. Both the PSFD- and~~ Profiles of S_{uu} obtained with the FV-based ~~solvers predict a spurious maximum $S_1 \approx 1$ at the first node off the wall, followed by a monotonic decrease in the $x_2/h \lessapprox 0.2$ range. The observed near-surface maximum may be originated from wall-blocking effects (Perot and Moin, 1995; Bae et al., 2018) such as splats, local regions of stagnation flow resulting from fluid impinging on a wall, investigated in Perot and Moin (1995) . Note that near-wall effects extend deeper within the boundary layer for the~~ solver in combination with the QUICK scheme and those from the simulations carried out with the PSFD-based solver are in good agreement with experimental results from Monty et al. (2009), which are here taken as a reference. The FV-based ~~runs and, further, the profiles remain positive~~

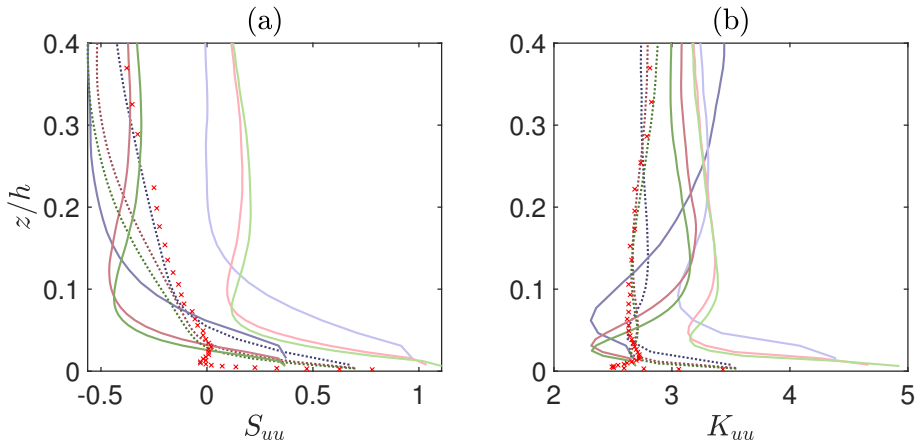

Figure 2. Vertical structure of skewness of streamwise velocity (a) ~~,~~ and kurtosis of streamwise velocity (b)~~and transfer efficiency coefficient (c)~~. Lines ~~and symbols~~ are defined in ~~Table 1~~Fig. 1. The red x-marks denote the measurements from Monty et al. (2009), digitalized by the authors.

~~throughout , except for the two coarse-resolution cases (C-2π and B-4π). Grid refinement in the horizontal directions improves the matching between the~~ solver, on the contrary, overpredicts S_{uu} when the linear interpolation scheme is used, with the skewness remaining positive throughout the whole extent of the surface layer. Note that a positive skewness of streamwise velocity represents a flow field where negative fluctuations are more likely to happen than the correspondent positive ones. The kurtosis obtained with the FV-based ~~and the PSFD-based solvers in the near-wall region, and accelerates the convergence of the profiles to the constant surface-layer values. K_1 profiles also feature a spurious maximum at the wall, and approximately constant values are reached above $x_2/h \approx 0.2$ for the B-2π, B-π, and F-2π cases, as well as for the R-2π case. On the contrary, no constant-K_1 layers are observed for the C-2π and B-4π cases. The constant-K_1 value~~ solver is consistently overpredicted, ~~signaling~~ representing a flow field ~~that is~~ populated by a ~~number of rare eventslarger than the one in real-world neutrally-stratified ABLs.~~ greater number of extreme events. Again, profiles from all cases featue a non-monotonic convergence to the reference ones, ~~From the transfer efficiency profiles shown in Fig. **??**(c) it is also apparent that both PSFD- and FV-based solvers predict a flow field populated by coherent structures that are more efficient in transferring momentum than those in measured ABLs (Bradshaw, 1967). The profiles from the FV-based solver reach an approximately constant r_{12} value further aloft ($x_2/h \approx 0.2$) when compared to the reference simulation R-2π~~as shown in Tab. 3, where the relative error on skewness and kurtosis with respect to the measurements from Monty et al. (2009) is reported, in the interval $z_0/h \leq z/h \leq 0.4$.

3.2 Spectra and autocorrelations

~~In this Sub-Section, spectra and spatial autocorrelations of the streamwise velocity fluctuations are analyzed, to quantify the distribution of energy density across scales and the spatial coherence of the simulated ABLs.~~

~~The one-dimensional spectrum of the~~

Table 3. ~~Average values of~~ Relative error on skewness ~~, kurtosis~~ $||S_{uu} - S_{uu,\mathrm{meas}}||_{L^2}/||S_{uu,\mathrm{meas}}||_{L^2}$ and ~~transfer efficiency coefficient~~ kurtosis $||K_{uu} - K_{uu,\mathrm{meas}}||_{L^2}/||K_{uu,\mathrm{meas}}||_{L^2}$ w.r.t. the measurements from Monty et al. (2009), in the interval ~~$0.2 \leq x_2/h \leq 0.4$~~ $z_0/h \leq z/h \leq 0.4$.

simulation	~~C-2π~~ FV64	~~B-4π~~ FV128	~~B-2π~~ FV160	~~B-π~~ FV64*	~~F-2π~~ FV1
~~$\langle S_1 \rangle_{surface\ layer}$~~ relative error on S_{uu}	~~−0.0660~~ 1.6339	~~−0.1566~~ 1.7656	~~−0.0013~~ 1.8142	~~0.1092~~ 0.8577	~~0.1509~~ 0.
relative error on K_{uu}	~~3.1223~~ 0.2832	~~3.2434~~ 0.2546	~~2.7480 $\langle r_{12} \rangle_{surface\ layer}$~~ 0.2538	~~0.4422~~ 0.2271	~~0.4169~~ 0.

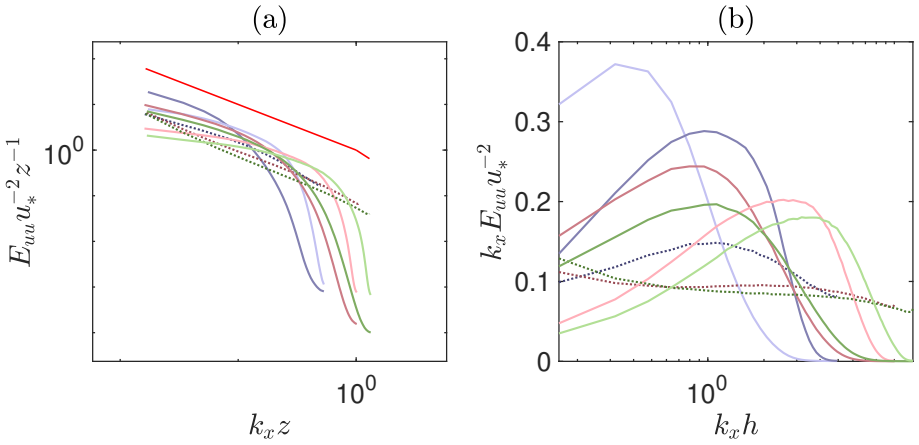

Figure 3. (a) Normalized one-dimensional spectrum of streamwise velocity at height $z/h \approx 0.1$. Solid red line, $(k_x z)^{-1}$ in the production range and $(k_x z)^{-5/3}$ in the inertial sub-range. All the other lines as in Fig. 1. (b) Premultiplied one-dimensional spectrum of streamwise velocity at $z/h \approx 0.1$.

One-dimensional spectra of streamwise velocity fluctuations (~~E_{11}) is featured~~ E_{uu}) for each of the considered cases are shown in Fig. ~~??~~3(a)~~for all of the considered cases. The profiles~~ . Profiles are contrasted against the phenomenological ~~production-range and inertial-sub-range~~ production range and inertial sub-range power-law profiles (k^{-1} and $k^{-5/3}$, respectively). Predictions from the PSFD-based solver feature a relatively good agreement with the phenomenological power-law profile, especially at the two highest grid resolutions, which feature a slope of -1.2 for the cases PSFD128 and PSFD160 in the production range (here defined as $k_x z < 1$). Profiles from the FV-based solver, on the contrary, exhibit strong sensitivity to grid resolution and are unable to capture the expected power-law behavior. ~~In the~~ In the production range, ~~the spectra are sensitive to the horizontal grid resolution, with an apparent decrease in the power-law exponent as the resolution is increased. The profiles from the simulations C-2π and B-4π and those from the simulations B-π and F-2π are similar, highlighting once again that the solution is more sensitive to the horizontal grid resolution than to the vertical one, and that the aspect ratio does not play an important role herein. In the high-wavenumber range, the profiles feature~~ velocity spectra from the FV solver start off relatively shallow at small wavenumbers, expecially when using the linear scheme. A narrow band where $E_{uu} \sim (k_x z)^{-1}$

can then be identified, followed by a rapid decay ~~of energy density, regardless of the resolution or the aspect ratio, and the decay is shifted towards higher wavenumber as the horizontal grid resolution is increased. Cases C-2π and B-4π also display an unphysical pile-up of energy near the cut-off frequency. It is evident that inertial-range turbulence dynamics may not be well captured~~ in energy density. The decay is especially pronounced when using the QUICK interpolation scheme, because of the associated numerical dissipation.

Overall, the energy density in the production range and in the ~~simulated cases, and this fact might complicate~~ inertial sub-range are not well captured by the FV-based solver and grid refinement does not help circumvent this limitation, at least at the considered resolutions. The authors note that this fact might limit the use of dynamic procedures based on the Germano et al. (1991) identity. ~~The results suggest that, for the considered resolutions, neither grid refinement nor the reduction of the aspect ratio help circumvent this limitation (no trend is observed). Note, however, that the contribution of the inertial-sub-range portion of the spectrum to the overall energy is modest, ranging from 10% to 15% for all the simulated cases (see Tab. **??**). On the contrary, predictions from the PSFD-based solver are not sensitive to grid resolution (not shown), and feature a very good agreement with the phenomenological $-5/3$ power-law profile in the inertial sub-range.~~

A further characterization of the energy ~~dynamics~~ distribution in the wavenumber space is given in Fig. **??**3(b), where ~~the premultiplied spectrum $k_1 h E_{11}/u_\tau^2$ is considered at selected heights for the cases F-2π and R-2π. Premultiplied spectra profiles~~ premultiplied velocity spectra $k_x E_{uu} u_\star^{-2}$ are shown. The usual reason for considering this quantity is to create a plot in semi-log scale where equal areas under the profiles correspond to equal energy. In addition, premultiplied spectra provide information on the coherence of the flow~~and~~ , in particular on the so-called ~~Large- and Very-Large- Scale Motions~~ large and very large scale motions (LSMs and VSLMs, respectively). ~~LSMs consist of single hairpin packets whose legs form counter-rotating rolls generating a low-velocity streamwise-elongated streak, also inducing high-momentum bulges on the sides of said streak. Velocity correlation analyses have shown that LSMs typically extend up to $3h$ in the streamwise direction and h in the spanwise direction. VLSMs arise due to clustering of such structures in the streamwise direction, and can reach streamwise extents of over $20h$ in boundary-layer flows.~~ These structures are responsible for carrying more than half of the kinetic energy and Reynolds shear stress and are a persistent feature of the surface and outer layers of both aerodynamically smooth and rough walls ~~(Hutchins and Marusic, 2007a; Fang and Porté-Agel, 2015). Numerous works have recently been devoted to the identification and characterization of LSMs and VLSMs in wall-bounded flows, both from a numerical and experimental perspective (Kim and Adrian, 1999; Balakumar and Adrian, 2007; Monty et al., 2007; Hutchins and Marusic, 2007b; Fang and Porté-Agel~~ (Kim and Adrian, 1999; Balakumar and Adrian, 2007; Monty et al., 2007; Hutchins and Marusic, 2007a; Fang and Porté-Agel, 2015). The current domain ~~, is~~ of modest dimensions ~~, can accommodate only~~ and should only be able to accommodate LSMs (Lozano-Durán and Jiménez, 2014), ~~commonly~~ which are identified in premultiplied spectra by a local maximum at the streamwise wavenumber ~~$k_1/h \approx 1$. As apparent from Fig. **??**(b), the premultiplied spectrum~~ $k_x/h \approx 1$. The location of the peaks from the FV-based solver ~~underpredicts the streamwise extent of LSMs~~with linear interpolation scheme shifts toward higher wavenumbers with grid refinement, with a maximum ~~located at $k_1/h \approx 3$. The PSFD-based solver~~ at $k_x/h \approx 4$ for the FV160 case. This signals a flow field where the streamwise extent of energetic modes (a.k.a., coherent structures) reduces as the grid is refined. The FV-based solver in combination with the QUICK scheme, on the contrary, ~~succeeds in capturing LSMs,~~

~~despite the modest~~ predicts the peak in premultiplied energy density at the expected wavenumber, hence suggesting that this approach is able to capture LSMs. The PSFD-based solver features a peak at the expected wavenumber ($k_x = 1$) only at the lowest resolution (PSFD64). Profiles from the higher resolution cases feature high energy densities at the lowest wavenumbers, highlighting an artificial "periodization" of energy-containing structures in the streamwise direction. This behavior is linked to the limited horizontal extent of the computational domain. The authors have indeed verified that a larged domain (twice as large along each horizontal direction) enables to capture LSM with the PSFD solver at resolutions matching that of the PSFD128 case (not shown). A corresponding single run of the FV solver was also carried out the said larger domain and premultiplied spectra were found to be in good agreement with those presented herein, supporting the working conjecture that the proposed domain size suffice to capture the range of variability of FV solvers for the problem under consideration.

~~(a) Normalized one-dimensional spectrum of streamwise velocity at height $x_2/h \approx 0.1$. Lines and symbols: solid red line, $(k_1 x_2)^{-1}$ in the production range and $(k_1 x_2)^{-5/3}$ in the inertial sub-range; for all the other lines and symbols please refer to Table 1. (b) Premultiplied one-dimensional spectrum of streamwise velocity from the simulations R-2π (full circles) and F-2π (solid lines). Dark to light gray lines correspond to heights from $x_2/h \approx 0.1$ to $x_2/h \approx 0.5$.~~

~~Ratio of inertial sub-range energy ($E_{inertial}$) to total energy (E_{total}) at $x_2/h \approx 0.1$. The the total energy is computed as the integral of the normalized spectrum across the whole available wavenumber range, whereas the inertial-range energy is obtained by integration in the wavenumber region with slope $-5/3$ or steeper.~~ ~~simulation C-2π B-4π B-2π B-π F-2π R-2π $E_{inertial}/E_{total}$ 0.1380 0.0951 0.1338 0.0947 0.1564 0.1188~~

~~To gain~~

To gain better insight on the spatial coherence of the flow field, the contour lines of the two-dimensional autocorrelation of the streamwise velocity ~~(R_{11}^{2D}) in the $x_1 x_3$~~ in the xy plane are shown in Fig. **??**~~.~~ 4. The $R_{uu} = 0.1$ contour is often used to identify the boundaries of coherent structures populating the flow field. ~~Contours from the F-2π case (Fig. **??**(b))~~ The contours from the FV-based solver with linear scheme (Figs. 4,a,d) are representative of a ~~flow field less correlated along both streamwise and spanwise directions than the one from the R-2π case~~ poorly correlated flow field, with a streamwise extent of the $R_{uu} = 0.1$ contour extending $0.5h$ and $0.1h$ in the streamwise and spanwise directions, respectively. On the contrary, the contours from the FV-based solver with QUICK scheme (Fig. **??**~~(a)),and also more isotropic (note that the scales in Fig. **??**(b) differ from those in Fig. **??**(a)). For example, the ellipse-shaped contour line at level 0.3 from the R-2π simulation is characterized by eccentricity $e \approx 0.9965$, while the corresponding value for the F-2π simulation is $e \approx 0.9473$.~~ 4,b,e) depict a flow field characterized by larger spatial autocorrelation, in line with results from the PSFD-based solver.

Note that the ~~quality of the computed flow statistics is not~~ flow statistics presented before should not be impacted by the fact that the current domain size prevents some of the contour lines ~~in the R-2π case~~ (simulations FV64*, FV160*, PSFD64, PSFD160) from closing (Lozano-Durán and Jiménez, 2014).

The one-dimensional ~~autocorrelation function (R_{11}~~spatial autocorrelation (R_{uu}), shown in Fig. **??** 5 along the streamwise and ~~spanwise coordinate directionsfor all of the considered cases, further supports the above statements. From the profiles from the R-2π simulation it is clear~~ cross-stream directions, further corroborates the above findings. From Fig. 5(a) it is apparent that the extension of the selected domain ~~is not suffiecient to capture all the dynamics, as R_{11}~~ does not enable the flow to

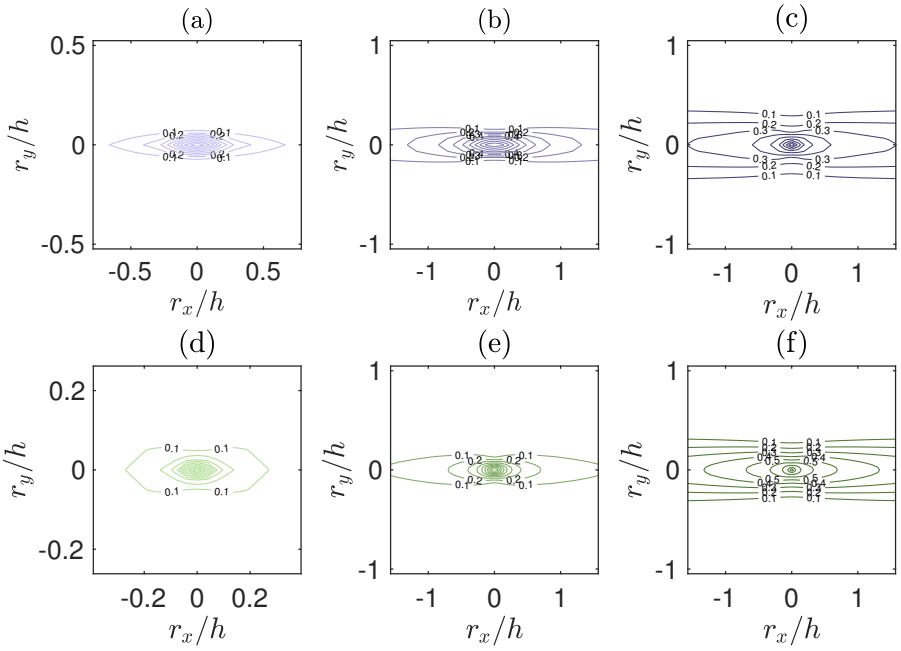

Figure 4. Contours of two-dimensional spatial autocorrelation of streamwise velocity at height $z/h \approx 0.1$, from the simulations FV64 (a), FV64* (b), PSFD64 (c), FV160 (d), FV160* (e) and PSFD160 (f). Contour levels from 0.1 to 0.9 with increments of 0.1.

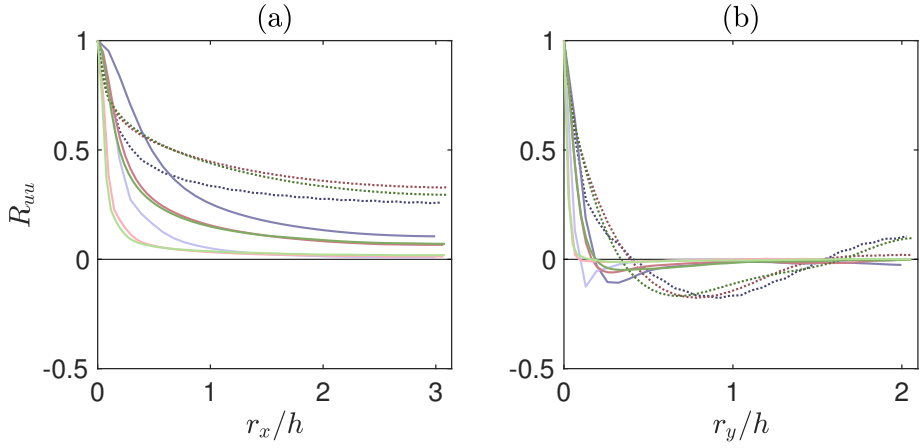

Figure 5. ~~Contours of two-dimensional~~ One-dimensional spatial autocorrelation of streamwise velocity at height ~~$x_2/h \approx 0.1$~~$z/h \approx 0.1$, ~~from~~ along the ~~simulation R-2π~~ streamwise direction (a) and ~~from~~ along the ~~simulation F-2π~~ cross-stream direction (b). ~~Dark to light gray lines correspond to contour levels from 0.1 to 0.9 with increments of 0.1~~Lines as in Fig. 1.

Table 4. Integral lengths at height ~~$x_2/h \approx 0.15$~~ $z/h \approx 0.15$.

simulation	~~C-2π~~ FV64	~~B-4π~~ FV128	~~B-2π~~ FV160	~~B-π~~ FV64*	~~F-2π~~ FV128*	~~R-2π~~ FV160*	PSFD64	PSI
~~$\Lambda_{r_1,u_1}/h$~~ $\Lambda_{r_x,u}/h$	~~0.5455~~ 0.2320	~~0.6496~~ 0.1203	~~0.2320~~ 0.1151	~~0.2637~~ 0.8246	~~0.1203~~ 0.5879	0.5930	1.2810	1.
~~$\Lambda_{r_3,u_1}/h$~~ $\Lambda_{r_y,u}/h$	~~0.0709~~ 0.0379	~~0.0708~~ 0.0293	~~0.0379~~ 0.0277	~~0.0415~~ 0.0967	~~0.0293~~ 0.0828	0.0828	0.1436	0.

become uncorrelated in the streamwise direction for the PSFD solver and for the FV solver using QUICK: R_{uu} remains finite in the available ~~r_1/h range . Along the spanwise direction , R_{11} features the~~ r_x/h range across resolutions. Profiles from the FV-based solver with using a linear interpolation, on the other hand, decay rapidly towards zero.

Along the cross-stream direction (Fig. 5,b), profiles from the PSFD-based solver feature the expected negative lobes, ~~which highlight~~ highlighting the presence of high- and low-momentum streamwise-elongated streaks flanking each others in ~~the streamwise direction,~~ said direction. This behavior is in line with findings from previous studies ~~focused~~ on the coherence of wall-bounded turbulence ~~. Throughout the considered~~ and with standard turbulence theory. Profiles from the FV-based solver ~~cases, R_{11} decays very rapidly along the streamwise and spanwise directions, more so as the grid is refined. Further, the negative lobesin the spanwise autocorrelation weaken in the B-π and F-2π cases , and spread over a much larger separation distance.~~ exhibit a similar profile, albeit featuring a more rapid decay and less prominent negative lobes, especially for the high-resolution cases using the linear interpolation scheme.

A quantitative measure of the coherence ~~length~~ of the flow field is provided in Tab.~~??~~ 4, where the integral lengths ~~Λ_{r_1,u_1} and Λ_{r_3,u_1} are reported , in a comparison with corresponding values from~~ $\Lambda_{r_x,u}$ and $\Lambda_{r_y,u}$ are reported for all the considered cases and for the direct numerical simulations of ~~the~~ a channel flow at $Re_\tau = 2000$ from Sillero et al. (2014). The integral ~~length Λ_{r_i,u_1} is obtained by integration of the R_{11} function along the i-th direction, from $r_i = 0$ to the first zero (if any) or to the closest intersection with $R_{11} = 0.05$, in line with the procedure outlined in Sillero et al. (2014) .~~ lengths in Tab. 4 are evaluated at $z/h \approx 0.15$, since the data from Sillero et al. (2014) were available at this height. ~~While Λ_{r_1,u_1} might be not meaningful for the R-2π case~~Although $\Lambda_{r_x,u}$ might not be meaningful across the considered cases, owing to the lack of a zero crossing of the autocorrelation function, it is apparent that the ~~values of the coherence lengths from the~~ FV-based solver ~~are much smaller than expected, and that the grid refinement procedure leads to a further reduction of both Λ_{r_1,u_1} and Λ_{r_3,u_1}. These findings highlight a flow field that is less correlated than realistic ABL flows, thus suggesting that the FV-based solver may not be capable of representing coherent structures– and associated momentum-transfer mechanisms– of ABL turbulence.~~

~~One-dimensional spatial autocorrelation of streamwise velocity at height $x_2/h \approx 0.1$, along the streamwise direction (a) and along the spanwise direction (b). Lines and symbols are defined in Table 1.~~

underestimates the integral lengths when compared to the PSFD cases and the reference DNS values, especially when the linear interpolation scheme is used.

3.3 ~~Instantaneous horizontal contours~~

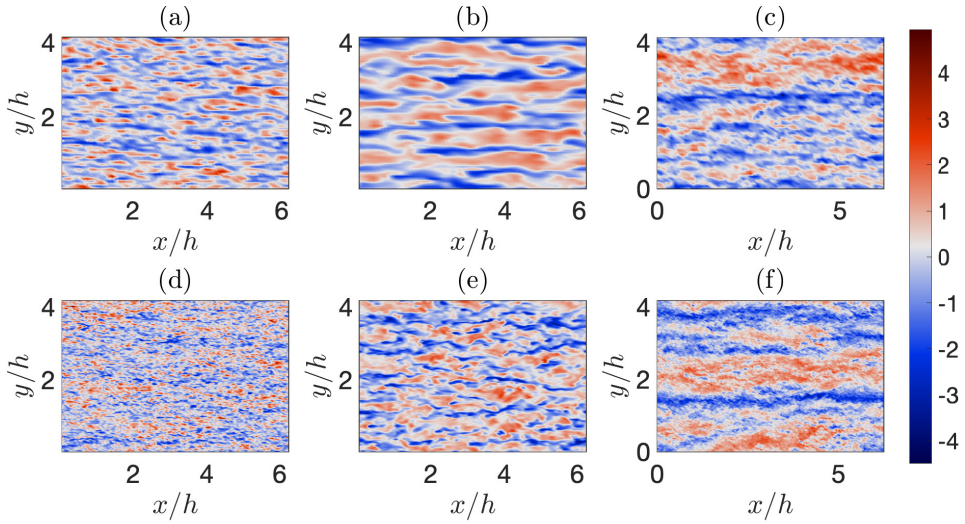

Figure 6. Instantaneous snapshots of normalized streamwise velocity fluctuations at $z/h \approx 0.1$ from the simulations FV64 (a), FV64* (b), PSFD64 (c), FV160 (d), FV160* (e) and PSFD160 (f). The normalized velocity fluctuation is defined as $(u - \langle u \rangle_{xy})/u''$, where averages (and fluctuations therefrom) are evaluated in space over the selected horizontal plane.

~~To further substantiate the lack of coherence in the FV flow fields, horizontal instantaneous snapshots of normalized~~ Instantaneous snapshots of streamwise velocity fluctuations ~~are shown in Fig. ?? for the simulations R-2π and F-2π. The normalized velocity fluctuation is defined as $(u_1 - \langle u_1 \rangle_{x_1 x_3})/u_1''$, where averages are carried out in space over the selected horizontal plane .~~ over a horizontal plane confirm said findings (see Fig. 6). ~~Streamwise-elongated~~ Artificially-periodized, streamwise-elongated bulges of uniform high and low momentum are indeed apparent in the ~~R-2π flow field~~ snapshots from the PSFD-based solver (Fig. **??**~~(a)~~6,c,f). ~~These are the typical flow patterns encountered in boundary-layer flows and have been the object of significant studies in both geophysics and engineering (Balakumar and Adrian, 2007; Hutchins and Marusic, 2007a; Fang and Porté-Agel, ~~ . The instantaneous streamwise velocity field from the ~~FV-based solver(Fig. ??(b)) exhibits a less coherent flow field when compared to the one from the PSFD-based solver. Differences are particularly stark in the spanwise direction, where thin structures populate the boundary layer and LSMs are not clearly detectable. To gain further insight on the problem, in the spirit of LES, the instantaneous velocity snapshots have been spatially low-pass filtered using a sharp-spectral-cut-off kernel with support $\ell_1/h \times \ell_3/h = 3x_2/h \times x_2/h$– approximately the extent of LSMs across the ABL (seeFig. ??(c) and (d)).~~ FV solver, on the contrary, appears to be populated by smaller regions of uniform momentum, especially when using the linear scheme and the size of energetic structures diminishes with increasing resolution (see, e.g., Figs. 6,a,d). ~~From the filtered flow field it is indeed apparent that larger-scale patterns are present in the OpenFOAM® solution, but these are less coherent than the corresponding ones from the PSFD-based solver, and energetically weaker, thus not bringing significant contributions to autocorrelation maps.~~

Instantaneous snapshots of normalized streamwise velocity fluctuations at $x_2/h \approx 0.1$ from simulations R-2π (a), F-2π (b), R-2π filtered (c) and F-2π filtered (d). The normalized velocity fluctuation is defined as $(u_1 - \langle u_1 \rangle_{x_1 x_3})/u_1''$, where averages (and fluctuations therefrom) are evaluated in space over the selected horizontal plane. A low-pass spatial filtering operation was carried out to obtain the flow field in panels (c) and (d), using a sharp-spectral-cut-off kernel with support $\ell_1/h \times \ell_3/h = 3x_2/h \times x_2/h$– approximately the extent of LSMs in the ABL.

3.3 Momentum transfer mechanisms

To elucidate the mechanisms responsible the for momentum transport in the flow, the conditionally-averaged flow field is analyzed, following the approach of Fang and Porté-Agel (2015). In Fig. **??**, a visualization of the conditionally-averaged flow field is provided– the conditional event being a positive streamwise velocity fluctuation u_1''/u_τ at $r_1/h = 0$, $x_2/h = 0.5$, $r_3/h = 0$. The flow structure in the equilibrium surface layer is expected to exhibit rolls in the vertical-spanwise plane, each roll flanked by a low- and a high-momentum streamwise-elongated streaks. The roll leads to sweep and ejection pairs, which occur in correspondence of This section is devoted to the high- analysis of momentum transfer mechanisms in the ABL, with a focus on quadrant analysis (Lu and Willmarth, 1973) and low-momentum streak respectively, and are the dominant mechanism responsible for tangential Reynolds stress (Ganapathisubramani et al., 2003; Lozano-Durán et al., 2012). The results from the simulation R-2π clearly capture said mechanism, with sweeps and ejections of the same order of magnitude. A qualitatively similar pattern can be obtained from the F-2π case, but streaks are significantly weaker when compared to those in the R-2π case (see details in caption of Fig. **??**). When the threshold is fixed to be the same as for the simulation R-2π, only positive-fluctuation patterns can be visualized, and the opposite occurs if the conditional event is a negative streamwise velocity fluctuation, signaling a flow field where a strong sweep (ejection) contributing to the tangential Reynolds stress does not have a corresponding ejection (sweep) pattern.

Conditionally-averaged flow field from the simulation R-2π ((a) and (c)) and from the simulation F-2π ((b) and (d)). The conditional event is a positive streamwise velocity fluctuation u_1''/u_τ at $r_1/h = 0$, $x_2/h = 0.5$, $r_3/h = 0$. Top: red iso-surfaces show $u_1''/u_\tau > 0.68$ (a) and $u_1''/u_\tau > 0.09$ (b); blue iso-surfaces show $u_1''/u_\tau < -0.54$ (a) and $u_1''/u_\tau < -0.04$ (b); vector fields in the spanwise-vertical planes are visualized at $r_1/h = -L_1/(4h), 0, L_1/(4h)$. Bottom: vector field in the spanwise-vertical plane at $r_1/h = 0$.

To gain further insight on relative contributions of sweeps and ejection to the overall Reynolds stress, a quadrant-hole analysis is proposed hereafter (Lu and Willmarth, 1973) . This technique is conditionally-averaged flow fields. The quadrant hole analysis is a technique based on the decomposition of the velocity fluctuations into four quadrants: the first and third quadrants, "outward interactions" *outward interactions* ($u' > 0$, $v' > 0$) and "inward interactions" $w' > 0$) and *inward interactions* ($u' < 0$, $v' < 0$)$w' < 0$), respectively, are negative contributions to the momentum flux, whereas the second and fourth quadrants, a.k.a. "ejections" *ejections* of low-speed fluid outward from the wall ($u' < 0$, $v' > 0$) and "sweeps" $w' > 0$) and *sweeps* of high-speed fluid toward the wall ($u' > 0$, $v' < 0 w' < 0$), represent positive contributions. The A range of flow statistics can be defined based on the said decomposition and used to provide insight on the mechanisms supporting momentum transfer in the ABL.

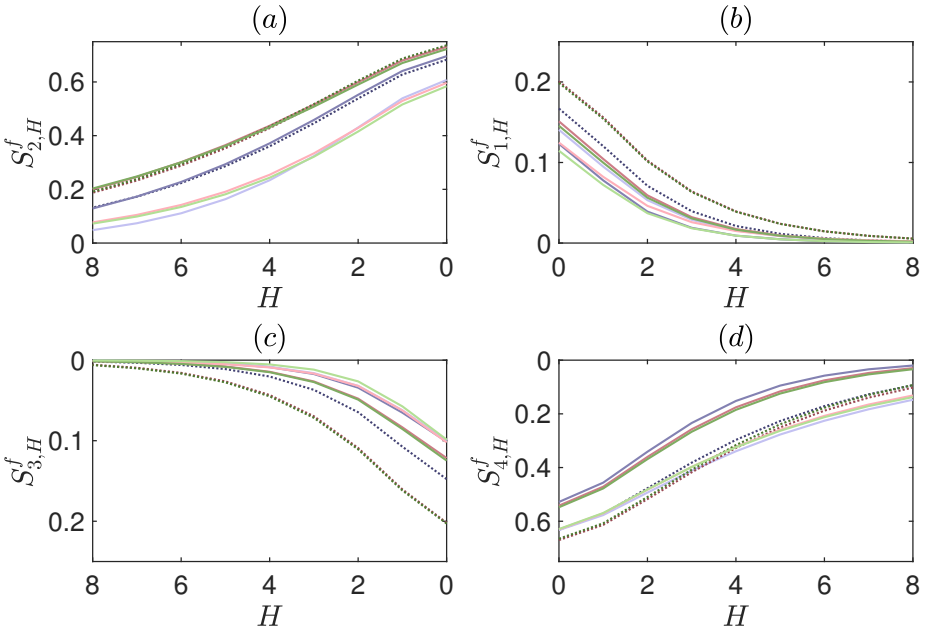

Figure 7. Stress fractions at $z/h \approx 0.1$. The profiles are normalized so that the sum of the stress fractions for $H = 0$ is unity across the cases. Lines are defined in Fig. 1.

Figure 7 features the quadrant-hole analysis, where the notation is the same as in Yue et al. (2007a), ~~where~~ with H ~~is~~ being the hole size, $S_{i,H}$ ~~is the~~ the resolved Reynolds shear stress contribution to the i-th quadrant at hole size H, and $S^f_{i,H}$ is the correspondent quadrant fraction. Stress fractions are presented for values of the hole size H ranging from 0 to 8, where larger hole sizes correspond to contributions to the resolved Reynolds shear stress from more extreme events. Clearly, the FV-based solver with the linear scheme underpredicts ejections (Fig. 7,a), outward interactions (Fig. 7,b) and inward interactions (Fig. 7,c), and overpredicts sweeps at large hole size H (Fig. 7,d). The QUICK scheme, on the contrary, predicts fairly well the magnitude of ejections (see Fig. 7,a) whereas profiles from the other quadrants are consistently underpredicted when compared to corresponding PSFD ones. It is well known that ejections are violent events, concentrated over a very thin region in the cross-stream direction of the ABL (Fang and Porté-Agel, 2015).

~~Figure ??~~To gain insight on the vertical structure of momentum transfer mechanisms Fig. 8(a) shows the exuberance ratio, defined as the ratio of negative to positive contributions to the momentum flux, $(S_{1,0}+S_{3,0})/(S_{2,0}+S_{4,0})$ (Shaw et al., 1983). ~~The magnitude of the profile from the R-2π simulation is larger than those from the FV runs, highlighting~~ Across the whole surface layer except for the first node at the wall, the exuberance ratios from the PSFD-based solver are larger (in absolute value) than the correspondent ones from the FV-based solver. The exuberance ratio profiles support findings from Fig. 7, which highlighted that outward and inward interactions have a ~~relative contribution to~~ significant impact on the resolved Reynolds stress ~~that is more significant for~~ in the PSFD-based solver, whereas the ~~FV results are characterized by relatively stronger~~

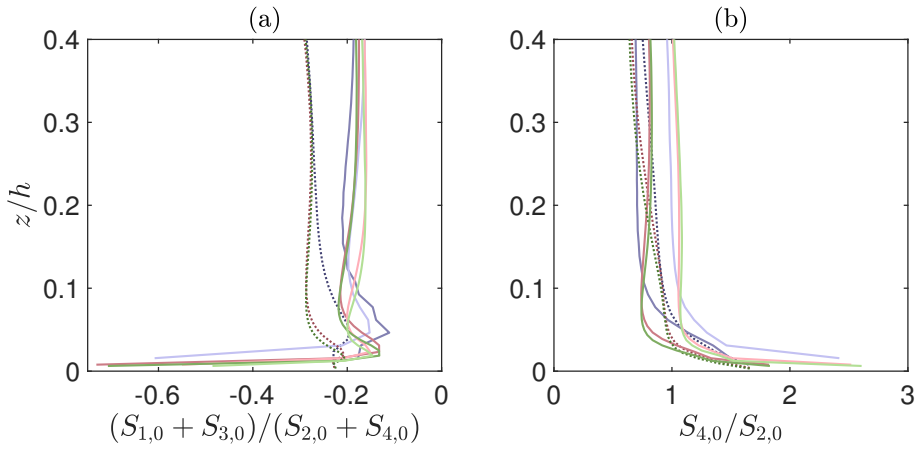

Figure 8. Vertical structure of event ratios: (a) ratio of negative to positive contributions to the momentum flux; (b) ratio of sweeps to ejections. Lines ~~and symbols are defined~~ as in ~~Table 1~~Fig. 1.

~~ejections and sweeps . More interestingly, from~~ flow simulated with the FV-based solver is characterized predominantly by sweeps and ejections. This behavior is consistent throughout the ABL. Fig. **??**8(b) ~~it is apparent that the FV solver tends to favor sweeps over ejection as the mechanisms for momentum transfer in the surface layer, which is at odds with the R-2π predictions~~ shows the ratio of sweeps to ejections in the lower portion of the ABL ($z/h \leq 0.4$). Profiles obtained with the QUICK scheme are in line with predictions from the PSFD-based solver and with findings from measurements of surface-layer flow over rough surfaces, ~~whereby~~ where ejections are identified as the dominant momentum transport mechanism ~~(Raupach et al., 1991)~~in the ABL (Raupach et al., 1991). On the contrary, the FV-based solver with linear scheme tends to favor sweeps over ejections as the mechanisms for momentum transfer in the surface layer, throughout the considered grid resolutions. ~~Grid refinement over the considered resolutions does not mitigate this shortcoming.~~

~~Consistently with these findings, the joint probability density function of~~ To conclude the analysis on the mechanisms responsible for momentum transfer, the conditionally-averaged flow field is discussed next. The approach of Fang and Porté-Agel (2015) is adopted to compute the conditionally-averaged flow field, where the conditional event is a positive streamwise velocity fluctuation u''/u_* at $\Delta x/h = 0$, $\Delta y/h = 0$, $z/h = 0.5$. Figure 9 features a pseudocolor and vector plot of the ~~streamwise and vertical velocity fluctuations for the simulation F-2π exhibits a narrower range of inner-outer interactions, as displayed in~~ conditionally-averaged velocity field in a cross-stream-vertical plane for selected cases whereas Fig. **??**~~(b). It is also apparent that the PSFD-based solver features a larger variance, highlighting that stronger sweeps and ejections are favored when compared to those from the FV-based solver.~~ 10 displays a three-dimensional iso-surface thereof.

~~Joint probability density function of the streamwise and vertical velocity fluctuations, normalized by the resolved Reynolds shear stress, at $x_2/h \approx 0.1$. Results from the simulation R-2π(a) and from the simulation F-2π (b).~~ The flow structure in the equilibrium surface layer is known to be characterized by counter-rotating rolls and low- and high-momentum streamwise-elongated

streaks flanking each others in the cross-stream direction. Rolls and streaks are indeed the dominant flow mechanism responsible for tangential Reynolds stress (Ganapathisubramani et al., 2003; Lozano-Durán et al., 2012).

These observations are further supported by As apparent from Fig. **??**, where stress fractions are reported for values of the hole size H ranging from 0 to 8. Note that larger hole sizes corresponds to contributions from more extreme events to the resolved Reynolds shear stress. Clearly, 9, the FV-based solver severely underpredicts ejections, outward interactions and inward interactions (PSFD conditionally-averaged velocity field exhibits counter-rotating patterns associated with positive and negative streamwise velocity fluctuations (corresponding to the aforementioned streaks). The roll modes feature a diameters $(d \approx h)$ throughout the ABL, which is consistent with findings from the literature, and positive an negative velocity fluctuations are approximately of the same magnitude $(\approx u_\tau)$. From Fig. **??**(a), (b) and (c), respectively), and slightly overpredicts extreme sweeps (Fig. **??**(d) at sufficiently large hole size H). This mismatch is particularly apparent for the low grid-resolution cases, with a general improvement as the grid is refined. Ejections in the ABL are known to be relatively violent events, concentrated over a very thin region in the spanwise direction (Fang and Porté-Agel, 2015). The findings from 10, it is also apparent how the considered isosurfaces extend in the streamwise direction for about $4h$. Quite surprisingly, the FV-based solver is not able to predict the roll modes, irrespective of the interpolation scheme or resolution, and the magnitude of the low-momentum streaks is also severely underpredicted across the considered cases. Further, Figs. 9 and 10 both depict a FV conditionally-averaged flow field that is poorly correlated in the cross-stream and streamwise directions, resulting in significantly smaller momentum-carrying structures. This supports previous findings from the two-point correlation maps (Fig. **??** suggest that , at 4).

The lack of roll modes implies that these solvers are not able to capture the fundamental mechanism supporting momentum transfer in the ABL, at least at the considered grid resolutions, the FV solver is not able to correctly capture said strong local events, leading to a less coherent flow field and, possibly, to many of the observed discrepancies with the R-2π case and with canonical ABL flow statistics. This limitation can also be identified as the root cause of several of the observed problematics with the FV solutions, including the relatively high (low) streamwise-velocity skewness when using using linear (QUICK) schemes (see Fig. 2,a) and the inbalance between sweeps and ejections (Fig. 1 and Fig. 8).

4 ~~Conclusion~~Conclusions

The objective of the present study was to determine whether second-order-accurate

This work provides insight on the quality and reliability of an important class of general-purpose, second-order accurate FV-based solvers are suitable for WMLESs of ABL flows. in wall-modeled LES of neutrally-stratified ABL flow. The FV solvers are part of the OpenFOAM® framework, make use of the divergence form of the nonlinear term, and are based on a colocated arrangement for the evaluation of the unknowns.

A suite of simulations has been carried out using a general-purpose co-located FV solver based on second-order centered schemes within the OpenFOAM® framework, varying parameters such as grid resolution and aspect ratio. Results in an open-channel flow setup, varying grid resolution (with grid refinement up to 160^3 control volumes), interpolation schemes

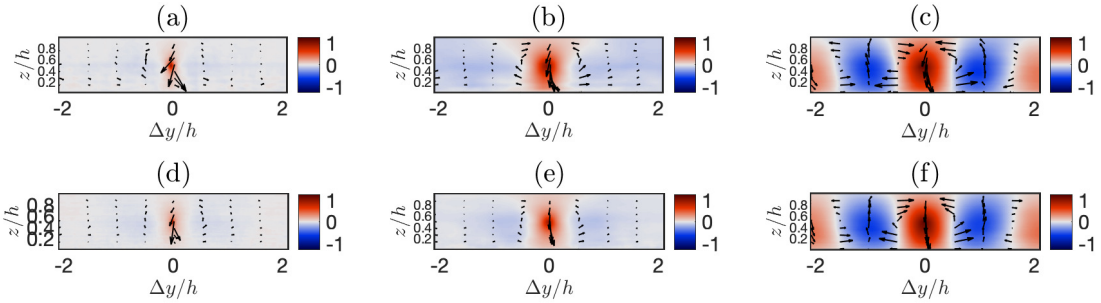

Figure 9. ~~Stress fractions~~ Visualization of the conditionally-averaged velocity field in the cross-stream-vertical plane at ~~$x_2/h \approx 0.1$~~$\Delta x/h = 0$ from simulations FV64 (a), FV64* (b), PSFD64 (c), FV160 (d), FV160* (e) and PSFD160 (f). ~~Profiles~~ Colors are ~~normalized so that~~ used to represent the ~~sum~~ magnitude of the ~~stress fractions for $H = 0$ is unity across~~ streamwise component, vectors denote the ~~cases. Lines~~ cross-stream and ~~symbols are defined~~ vertical components. The conditional average is computed as in ~~Table 1~~Fig. 10.

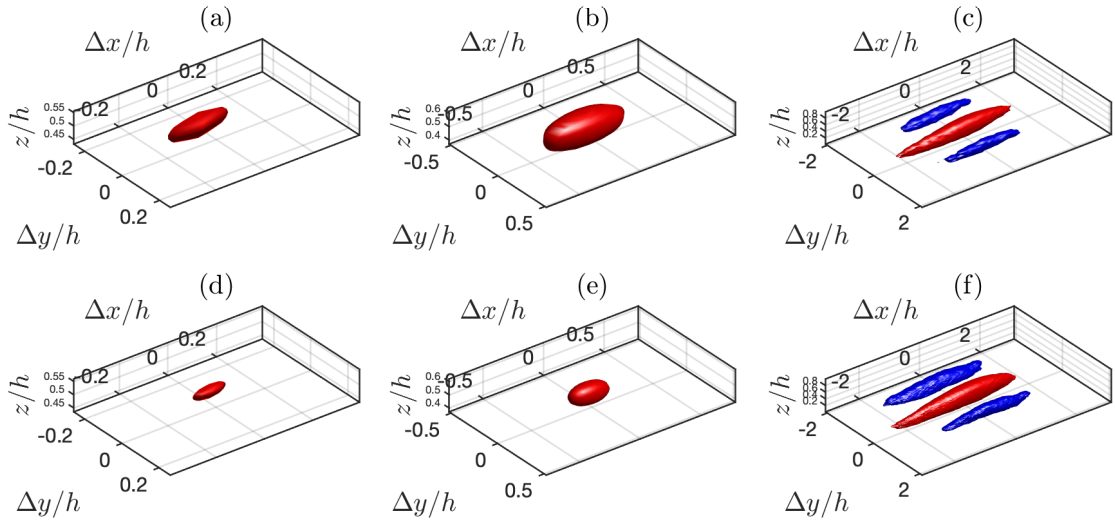

Figure 10. Conditionally-averaged flow field from simulations FV64 (a), FV64* (b), PSFD64 (c), FV160 (d), FV160* (e) and PSFD160 (f). The conditional event is a positive streamwise velocity fluctuation u''/u_* at $\Delta x/h = 0$, $\Delta y/h = 0$, and $z/h = 0.5$. Red iso-surfaces show $u''/u_* > 0.7$ (top) and $u''/u_* > 0.65$ (bottom); blue iso-surfaces show $u''/u_* < -0.55$ (top) and $u''/u_* < -0.5$ (bottom).

for the discretization of the nonlinear term (linear and QUICK), the value of the Smagorinsky coefficient ($C_S = 0.1$ to $C_S = 1.678$), the pressure-velocity coupling method and the time-advancement scheme (PISO with a second order Adams-Moulton and a projection method with a fourth order Runge-Kutta time stepping scheme). Several flow statistics have been contrasted against ~~those from a validated~~ profiles from a well established PSFD-based solver ~~.~~

~~Mean velocity and resolved Reynolds stresses are found to be particularly sensitive to variations in the surface-parallel grid resolution, and a relatively good convergence to corresponding profiles from the PSFD-based solver has been observed as the grid is refined. On the contrary, higher-order velocity statistics,~~ and against experimental measurements (when the latter were available). Considered flow statistics include the mean velocity, turbulence intensities, velocity skewness and kurtosis, velocity spectra and spatial autocorrelations~~are severely mispredicted across grid resolutions. Skewness, kurtosis, and transfer efficiency coefficient are not constant in the surface layer (i.e., the flow is not self-similar) and are consistently overpredicted therein. Streamwise velocity spectra exhibit no phenomenological production range, are very sensitive to variations in the grid resolution and aspect ratio, and decay too rapidly in the inertial sub-range as a result of truncation errors. Further, the spectral peaks in the premultiplied streamwise velocity spectra are shifted to higher wavenumber when compared to the reference PSFD solution, and the corresponding spatial autocorrelation of the streamwise velocity rapidly decays across the ABL along both the streamwise and spanwise coordinate directions. Consistently with these findings, instantaneous snapshots of~~ . An analysis of mechanisms supporting momentum transfer in the flow field has also been proposed. Main findings are summarized below.

With the exception of the FV solver based on the projection and Runge-Kutta time advancement scheme, mean velocity profiles from the PSFD and FV solvers feature a positive LLM and existing techniques to alleviate this limitation lead to no apparent improvements. This observation suggests that, for this class of solvers, alternative approaches should be devised to overcome this limitation in ABL flow simulations.

Near-surface streamwise velocity fluctuations are consistently overpredicted by both the PSFD and FV solvers, irrespective of the grid resolution. The overshoot is particularly pronounced for the cases based on the QUICK interpolation scheme. This behavior can be related to a deficit of pressure redistribution in the budget equations for the velocity variances, which results in a pile up of shear-generated streamwise velocity fluctuations ~~reveal that the flow is populated by shorter and thinner structures. The dominant mechanism supporting the tangential Reynolds stress in ABL flow – spanwise-paired sweeps and ejections– is found to be much weaker than what commonly observed in the ABL, with sweeps dominating over ejections in the~~ and deficit in the vertical and cross-stream velocity fluctuation components.

The interpolation scheme used for the discretization of the nonlinear term plays a role in determining the remaining flow statistics. Specifically, FV solvers using a linear interpolation scheme lead to i) a positive streamwise velocity skewness throughout the surface layer, which is at odds with ~~available measurements and with corresponing results from the PSFD-based solver. A quadrant-hole analysis highlighted how the considered FV-based solver severely underpredicts ejection events, which are notoriously localized in the spanwise direction, as well as inner and outer interactions. In the authors' opinion, this underprediction of ejection events is the root-canse of many of the observed mismatches and sensitivity to grid resolution of flow statistics. This statement is partly supported by the strong sensitivity of quadrant profiles to~~ experimental findings; ii) a severe overprediction of the streamwise velocity kurtosis; iii) a poorly correlated streamwise velocity field in the horizontal directions, especially at high grid resolutions; iv) a severe underprediction of outward and inward interactions and ejection events; and v) a lack of high- and low-momentum streaks paired with roll modes in the conditionally-averaged flow field. Grid resolution is either not affecting the above quantities or leading to larger departures from the reference profiles.

When the QUICK scheme is used, the ~~grid stencil, and to the approximately monotonic convergence of ejection ($S^f_{2,H}$)~~ ~~profiles towards the reference PSFD ones~~ i) streamwise velocity skewness is better predicted when compared to the linear scheme and profiles show a convergence towards reference experimental measurements; ii) the kurtosis of the streamwise velocity is also better predicted, especially as the grid ~~is refined~~stencil is reduced; iii) the streamwise velocity field feature a higher degree of correlation when compared to those from the linear scheme in the horizontal directions, but integral length scales are still only a fraction of those from the PSFD and reference DNS results; iv) outward and inward interactions and sweep events are severely underpredicted; and v) there is again lack of organized high- and low-momentum streaks and roll modes in the conditionally-averaged flow field.

~~Overall, the present findings show that truncation errors have an overwhelming impact on the predictive capabilities of second-order-accurate~~ To summarize, the considered class of FV-based solvers ~~that rely on a co-located grid set-up and centered schemes for the WMLES of ABLflow~~overall predicts a flow field that is less correlated in space when compared that of the PSFD solver and is not able to capture the salient features responsible for momentum transfer in the ABL, at least at the considered grid resolutions. These limitations appear to be the root cause of many of the observed discrepancies between FV flow statistics and the reference PSFD or experimental ones, including the mispredicted streamwise-velocity skewness (Fig. 2,a), the inbalance between sweeps and ejections (Fig. 1 and Fig. 8), and the overall sensitivity of flow statistics to variations in the grid resolution. ~~Although first- and second-order statistics can be considered acceptable provided sufficient grid resolution, the predictive capabilities of said solvers are relatively poor for~~

Findings from this study indicate that higher grid resolutions—or a different arrangement of the computational grid—might be required to correctly capture the aforementioned quantities and achieve resolution-independent results in wall-modeled LES of neutrally-stratified ABLs. Given that grid resolutions used herein are state-of-the-art for general purpose FV-based solvers and that computing power increases relatively slowly with time (Moore, 1965), the aforementioned limitations are likely to persist for years to come and introduce a degree of uncertainty in model results that needs to be addressed. This calls for further research aimed at reducing the impact of discretization and modeling errors, such as introducing discretizations that rely on staggered grid arrangements or using higher-order ~~statistics, velocity spectra, and turbulence topology.~~ spatial-discretization schemes.

Code availability. OpenFOAM® is an open-source computational fluid dynamics toolbox. The present study features the OpenFOAM® version 6.0, available for download at https://openfoam.org/version/6/. The Matlab scripts used for the post-processing are accessible from the GitLab repository https://gitlab.com/turbulence-columbia/miscellaneous/fv-solvers-abl-flow.

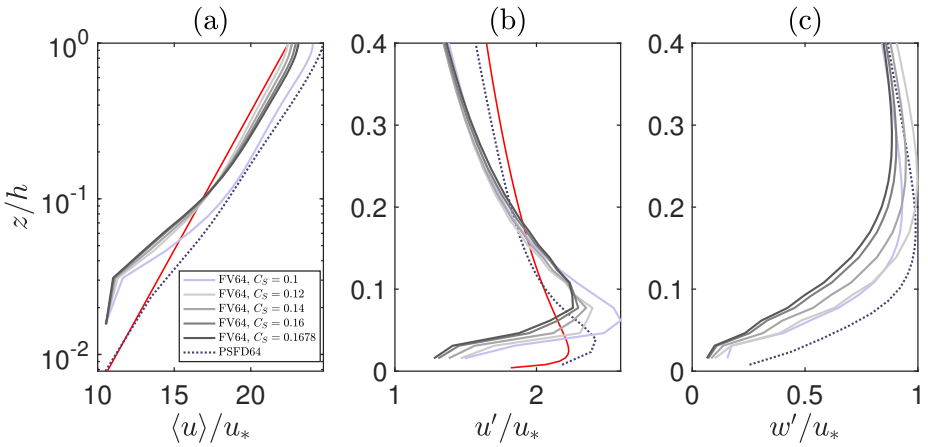

Figure A1. Vertical structure of streamwise velocity (a), streamwise velocity RMS (b), vertical velocity RMS (c). ~~Circles~~Red lines denote the phenomenological logarithmic-layer profile (a) and the analytical expressions from similarity theory (Stull, 1988) (b, ~~dark to light gray, $C_S = 0.1$ to $C_S = 0.1678$; full circles, PSFD~~c).

Appendix A

A1 Smagorinsky constant

A sensitivity analysis on the Smagorinsky constant C_S is here performed~~, considering~~. In addition to $C_S = 0.1$, the values $C_S = 0.12$, $C_S = 0.14$, $C_S = 0.16$, and $C_S = 0.1678$ (the default value in OpenFOAM®) are considered. All the tests are run on 64^3 control volumes.

As shown in Fig. A1(a), ~~C_S~~ the Smagorinsky constant has an impact on the ~~LLM, whereby the $C_S = 0.1$ case~~ mean streamwise velocity profile. The case at $C_S = 0.1$ results in the largest positive LLM, in agreement with the predictions from the ~~PSFD solver, and larger values of the coefficient predict~~ PSFD-based solver, whereas the cases at larger C_S exhibit a smaller, albeit still positive, LLM. The Smagorinsky coefficient has a discernible impact on the velocity RMSs. Specifically, the magnitude of the near-surface maximum ~~in both u'_1~~ for both u' (Fig. A1~~(b)) and u'_2~~,b) and w' (Fig. A1~~(c))~~,c) is reduced, and ~~its location~~ the location of the maximum is shifted away from the ~~surface– likely~~ surface—possibly the result of a higher near-surface energy dissipation as C_S is increased. ~~Larger C_S values also~~ In addition, larger values of C_S yield a more apparent departure from ~~corresponding profiles from~~ the corresponding profiles obtained with the PSFD-based solver.

~~One-dimensional~~ The one-dimensional spectra (Fig. A2~~(a))~~,a) show that larger ~~C_S coefficients~~ values of the Smagorinsky coefficient result in a more rapid decay of energy density ~~throughout the spectrum,~~ and in a shift of profiles ~~in~~ toward the inertial sub-range. Interestingly, ~~such profiles are characterized by the same~~ all the profiles exhibit the same slope, hence the same power-law exponent. No value of the Smagorinsky coefficient seems ~~able to yield a~~ suitable for capturing the $k^{-5/3}$ power law in the inertial sub-range. ~~Further, as also shown in Fig. A2(b) and (c), increasing~~ Increasing C_S ~~when compared to~~

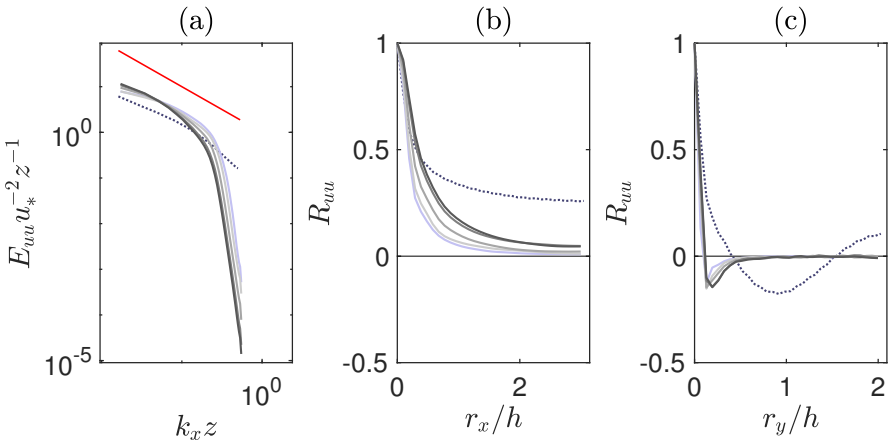

Figure A2. ~~Vertical structure~~ Normalized one-dimensional spectrum of streamwise velocity at height $z/h \approx 0.1$ (a)~~,~~ ; one-dimensional spatial autocorrelation of streamwise velocity ~~RMS~~ at height $z/h \approx 0.1$ along the streamwise direction (b) ~~, vertical velocity RMS~~ and along the cross-stream direction (c). ~~Circles~~Lines as in Fig. A1. Red line, ~~linear interpolation scheme; x-marks, QUICK interpolation scheme; full circles, PSFD~~$(k_xz)^{-1}$.

~~the considered value~~ leads to a modest improvement ~~on the R_{11} profiles , with no impact on the previously drawn conclusions.~~

~~Normalized one-dimensional spectrum of streamwise velocity at height $x_2/h \approx 0.1$ (a); one-dimensional spatial autocorrelation of streamwise velocity at height $x_2/h \approx 0.1$ along the streamwise direction (b) and along the spanwise direction (c). Circles, dark to light gray, $C_S = 0.1$ to $C_S = 0.1678$; full circles, PSFD; solid red line, $(k_1x_2)^{-1}$ in the production range and $(k_1x_2)^{-5/3}$ in the inertial sub-range.~~

A2 ~~Interpolation schemes~~

~~The results in §3 made use of the linear interpolation scheme to evaluate the terms in the filtered Navier-Stokes equations at the face-centers, as a consequence of the Gauss divergence theorem. Additional tests were carried out using the QUICK interpolation scheme (Ferziger and Peric, 2002) for the evaluation of non-linear terms, and results thereof are here compared with the R-2π and B-2π cases, at the same grid resolution.~~

~~Figure **??**(a) shows the vertical structure of the mean streamwise velocity.The QUICK and the linear schemes provide the same results in the near-wall region,where an underprediction is observed (see LLM). The interpolation scheme plays a role in the outer layer, where the velocity profile obtained with the QUICK scheme shows a speed-up when compared to the R-2π and B-2π cases. The RMSs of streamwise and vertical velocities are shown in~~ in the profiles of the spatial autocorrelation (Fig. A2,b and Fig. ~~**??**(b) and (c), respectively. In the near-wall region, an overprediction of u_1' and an underprediction of u_2' characterize the FV results, more severe when the QUICK scheme is used.~~ A2,c).

~~The one-dimensional spectrum, shown in Fig. **??**(a), exhibits the k^{-1} power-law behavior typical of the production range at low wavenumber. In the inertial sub-range, the profile obtained with the QUICK scheme decays faster than the one from the B-2π case, and the decay starts at lower wavenumbers. In terms of one-dimensional spatial autocorrelation (Fig. **??**(b) and (c)), the QUICK interpolation scheme performs slightly better than the linear one, in the sense that the decay of the autocorrelation is slower.~~

~~Normalized one-dimensional spectrum of streamwise velocity at height $x_2/h \approx 0.1$ (a); one-dimensional spatial autocorrelation of streamwise velocity at height $x_2/h \approx 0.1$ along the streamwise direction (b) and along the spanwise direction (c). Circles, linear interpolation scheme; x-marks, QUICK interpolation scheme; full circles, PSFD.~~

~~The instantaneous snapshot of the streamwise velocity fluctuations proposed in Fig. **??**, obtained with the QUICK scheme, highlights that the flow field features larger (more coherent) patterns when compared to those shown in Fig. **??**.~~

~~Instantaneous snapshot of streamwise velocity fluctuations, as defined in Fig. **??**, at height $x_2/h \approx 0.1$.~~

A2 ~~`rk4projectionFoam`~~Solvers

In this Sub-Appendix, an alternative solver ~~in~~ within the OpenFOAM® framework is considered, and the results are contrasted against those ~~obtained with `pisoFoam`. The solver, `rk4projectionFoam`,~~ previously shown (obtained with the PISO algorithm in combination with an Adams–Moulton time-advancement scheme). The solver is based on a projection method coupled with the ~~Runge-Kutta~~ Runge–Kutta 4 time-advancement scheme (Ferziger and Peric, 2002). Details on the implementation can be found in Vuorinen et al. (2015) (note that, in their reported code, a term in the form of a ~~time-step~~ time step Δt is missing, leading to a dimensional mismatch and raising a ~~compile-time~~ compile time error). ~~A comparison of the~~ The performances of the ~~solvers has been performed~~ two solvers have already been compared at moderate Reynolds number in Vuorinen et al. (2014), where it is pointed out that ~~`rk4projectionFoam`~~ the projection method coupled with the Runge–Kutta 4 time advancement scheme provides similar results at lower computational cost~~when compared to `pisoFoam`.~~. In the following, the performances of the solver are tested at high Reynolds number ($Re_\tau = 10^7$). ~~The same cases simulated with `pisoFoam` (Table 1)~~ Two simulations, over 64^3 cubes (case FV64RKp) and over 128^3 cubes (case FV128RKp), are considered.

In Fig. A3(a) the vertical profile of the mean streamwise velocity is shown. The ~~`rk4projectionFoam`~~ use of the projection Runge–Kutta 4 solver leads to ~~a behavior that is similar to the `pisoFoam` one in the very near surface region, but~~ an underprediction of the velocity at the wall as for the simulations FV64 and FV128. Interestingly, the profiles feature no LLM in the surface layer. ~~Streamwise~~ The streamwise and vertical velocity RMSs~~are~~, shown in Fig. A3(b) and Fig. A3(c), ~~respectively. The same scenario as the one obtained with `pisoFoam` is observed: turbulence intensities are underpredicted~~ exhibit the behavior already analyzed in §3.1, with an underprediction in the near-wall region, ~~$u_1'^+$ peak values are overpredicted and $u_2'^+$ peak values are underpredicted (except for the cases B-π and F-2π)~~an overpredition of the u'^+ peak and an underprediction of the w'^+ peak.

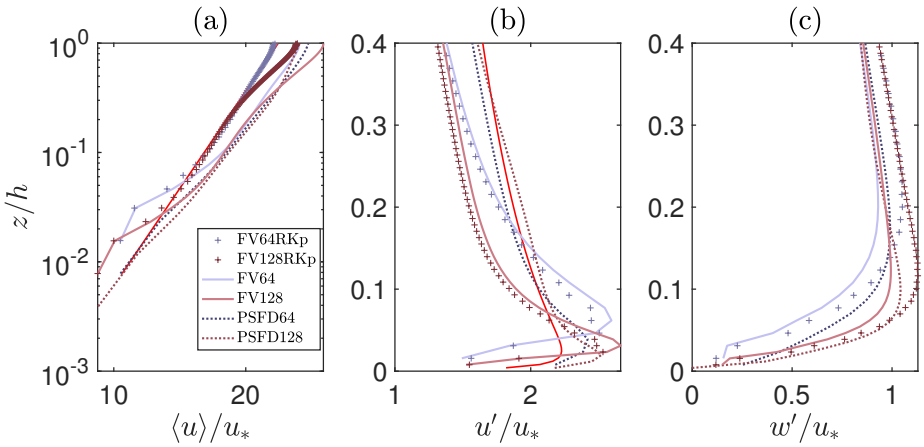

Figure A3. Vertical structure of streamwise velocity (a), streamwise velocity RMS (b), vertical velocity RMS (c). ~~Lines~~ Red lines denote the phenomenological logarithmic-layer profile (a) and ~~symbols are defined in Table 1~~the analytical expressions from similarity theory (Stull, 1988) (b, c).

Author contributions. BG and MG designed the study, BG conducted the analysis under the supervision of MG, BG and MG wrote the manuscript.

Competing interests. The authors declare that they have no conflict of interest.

Acknowledgements. The work was supported via start-up funds provided by the Department of Civil Engineering and Engineering Mechanics at Columbia University. The authors acknowledge computing resources from Columbia University's Shared Research Computing Facility project, which is supported by NIH Research Facility Improvement Grant 1G20RR030893-01, and associated funds from the New York State Empire State Development, Division of Science Technology and Innovation (NYSTAR) Contract C090171, both awarded April 15, 2010. The authors are grateful to Weiyi Li for generating the PSFD data, and to Drs. Ville Vuorinen and George I. Park for useful discussions on the performance of ~~Finite-Volume-based~~ finite-volume based solvers for the simulation of turbulent flows.

References

Abkar, M. and Porté-Agel, F.: The effect of free-atmosphere stratification on boundary-layer flow and power output from very large wind farms, Energies, 6, 2338–2361, 2013.

Albertson, J. and Parlange, M.: Natural integration of scalar fuxes from complex terrain, Adv. Water Resour., 23, 239–252, 1999.

Anderson, W. and Meneveau, C.: A large-eddy simulation model for boundary-layer flow over surfaces with horizontally resolved but vertically unresolved roughness elements, Bound.-Layer Meteorol., 137, 397–415, 2010.

Bae, H., Lozano-Durán, A., Bose, S., and Moin, P.: Turbulence intensities in large-eddy simulation of wall-bounded flows, Phys. Rev. Fluids, 3, 2018.

Bailey, B. and Stoll, R.: Turbulence in sparse, organized vegetative canopies: a large-eddy simulation study, Bound.-Layer Meteorol., 147, 369–400, 2013.

Balakumar, B. and Adrian, R.: Large- and very-large-scale motions in channel and boundary-layer flows, Phil. Trans. R. Soc. A, 365, 665–681, 2007.

Balogh, M., Parente, A., and Benocci, C.: RANS simulation of ABL flow over complex terrains applying an enhanced k-ϵ model and wall function formulation: implementation and comparison for fluent and OpenFOAM, J. Wind Eng. Ind. Aerodyn., 2012.

Beaudan, P. and Moin, P.: Numerical experiments on the flow past a circular cylinder at sub-critical Reynolds number, Tech. rep., Thermosciences Div., Stanford University, California, 1994.

Bose, S. and Moin, P.: A dynamic slip boundary condition for wall-modeled large-eddy simulation, Phys. Fluids, 26, 2014.

Bose, S. and Park, G.: Wall-modeled large-eddy simulation for complex turbulent flows, Annu. Rev. Fluid Mech., 50, 535–561, 2018.

Bou-Zeid, E., Meneveau, C., and Parlange, M.: A scale-dependent Lagrangian dynamic model for large eddy simulation of complex turbulent flows, Phys. Fluids, 17, 2005.

Bou-Zeid, E., Overney, J., Rogers, B., and Parlange, M.: The effects of building representation and clustering in large-eddy simnulations of flows in urban canopies, Bound.-Layer Meteorol., 132, 415–436, 2009.

Bradshaw, P.: 'Inactive' motion and pressure fluctuations in turbulent boundary layers, J. Fluid Mech., 30, 241–258, 1967.

Breuer, M.: Large eddy simulation of the subcritical flow past a circular cylinder: numerical and modeling aspects, Int. J. Numer. Meth. Fluids, 28, 1281–1302, 1998.

Calaf, M., Meneveau, C., and Meyers, J.: Large eddy simulation study of fully developed wind-turbine array boundary layers, Phys. Fluids, 22, 2010a.

Calaf, M., Meneveau, C., and Meyers, J.: Large eddy simulation study of fully developed wind-turbine array boundary layers, Phys. Fluids, 22, 2010b.

Canuto, C., Hussaini, M., Quarteroni, A., and Zang, T.: Spectral methods: fundamentals in single domains, Springer, 2006.

Chamecki, M.: Persistence of velocity fluctuations in non-Gaussian turbulence within and above plant canopies, Phys. Fluids, 25, 2013.

Chen, F., Kusaka, H., Bornstein, R., Ching, J., Grimmond, C., Grossman-Clarke, S., Loridan, T., Manning, K., Martilli, A., Miao, S., Sailor, D., Salamanca, F., Taha, H., Tewari, M., Wang, X., Wyszogrodzki, A., and Zhang, C.: The integrated WRF/urban modelling system: development, evaluation, and applications to urban environmental problems, Int. J. Climatol., 31, 273–288, 2011.

Cheng, W. and Porté-Agel, F.: Evaluation of subgrid-scale models in large-eddy simulation of flow past a two-dimensional block, Int. J. Heat Fluid Flow, 44, 301–311, 2013.

Chester, S., Meneveau, C., and Parlange, M.: Modeling turbulent flow over fractal trees with renormalized numerical simulation, J. Comput. Phys., 225, 427–448, 2007a.

Chester, S., Meneveau, C., and Parlange, M.: Modeling turbulent flow over fractal trees with renormalized numerical simulation, J. Comput. Phys., 225, 427–448, 2007b.

Chow, F., Street, R., Xue, M., and Ferziger, J.: Explicit filtering and reconstruction turbulence modeling for large-eddy simulation of neutral boundary layer flow, J. Atmos. Sci., 62, 2058–2076, 2005.

Churchfield, M., Vijayakumar, G., Brasseur, J., and Moriarty, P.: Wind energy-related atmospheric boundary layer large-eddy simulation using OpenFOAM, Presented as Paper 1B.6 at the American Meteorological Society, 19^{th} Symposium on Boundary Layers and Turbulence NREL/CP-500-48905, National Renewable Energy Laboratory, Colorado, 2010.

Churchfield, M., Lee, S., and Moriarty, P.: Adding complex terrain and stable atmospheric condition capability to the OpenFOAM-based flow solver of the simulator for on/offshore wind farm applications (SOWFA), Presented at the 1^{st} symposium on OpenFOAM in Wind Energy, Oldenburg, Germany, National Renewable Energy Laboratory, 2013.

De Villiers, E.: The potential for large eddy simulation for the modeling of wall bounded flows, Ph.D. thesis, Imperial College of Science, Technology and Medicine, 2006.

Deardorff, J.: A numerical study of three-dimensional turbulent channel flow at large Reynolds numbers, J. Fluid Mech., 41, 453–480, 1970.

Del Álamo, J., Jiménez, J., Zandonade, P., and Moser, R.: Self-similar vortex clusters in the turbulent logarithmic region, J. Fluid Mech., 561, 329–358, 2006.

Fang, J. and Porté-Agel, F.: Large-eddy simulation of very-large-scale motions in the neutrally stratified atmospheric boundary layer, Bound.-Layer Meteorol., 155, 397–416, 2015.

Fang, J., Diebold, M., Higgins, C., and Parlange, M.: Towards oscillation-free implementation of the immersed boundary method with spectral-like methods, J. Comput. Phys., 230, 8179–8191, 2011.

Fernando, H.: Fluid dynamics of urban atmospheres in complex terrain, Ann. Rev. Fluid Mech., 42, 365–389, 2010.

Ferziger, J. and Peric, M.: Computational methods for fluid dynamics, Springer, 2002.

Ganapathisubramani, B., Longmire, E., and Marusic, I.: Characteristics of vortex packets in turbulent boundary layers, J. Fluid Mech., 478, 35–46, 2003.

García-Sánchez, C., Tendeloo, G. V., and Gorlé, C.: Quantifying inflow uncertainties in RANS simulations of urban pollutant dispersion, Atmos. Environ., 161, 263–273, 2017.

García-Sánchez, C., van Beeck, J., and Gorlé, C.: Predictive large eddy simulations for urban flows: challenges and opportunities, Build. Environ., 139, 146–156, 2018.

Germano, M., Piomelli, U., Moin, P., and Cabot, W.: A dynamic subgrid-scale eddy viscosity model, Phys. Fluids, 3, 1991.

Ghosal, S.: An analysis of numerical errors in large-eddy simulations of turbulence, J. Comput. Phys., 125, 187–206, 1996.

Giometto, M., Christen, A., Egli, P., Schmid, M., Tooke, R., Coops, N., and Parlange, M.: Effects of trees on mean wind, turbulence and momentum exchange within and above a real urban environment, Adv. Water Resour., 106, 154–168, 2017.

Hultmark, M., Calaf, M., and Parlange, M.: A new wall shear stress model for atmospheric boundary layer simulations, J. Atmos. Sci., 70, 3460–3470, 2013.

Hutchins, N. and Marusic, I.: Large-scale influences in near-wall turbulence, Phil. Trans. R. Soc. A, 365, 647–664, 2007a.

Hutchins, N. and Marusic, I.: Evidence of very long meandering features in the logarithmic region of turbulent boundary layers, J. Fluid Mech., 579, 1–28, 2007b.

Issa, R.: Solution of the implicitly discretised fluid flow equations by operator-splitting, J. Comput. Phys., 62, 40–65, 1985.

Jasak, H., Jemcov, A., and Tukovic, Z.: OpenFOAM: A C++ library for complex physics simulations, Presented at the International Workshop on Coupled Methods in Numerical Dynamics, IUC, Dubrovnik, Croatia, 2007.

Kawai, S. and Larsson, J.: Wall-modeling in large eddy simulation: length scales, grid resolution, and accuracy, Phys. Fluids, 24, 2012.

Kim, K. and Adrian, R.: Very large-scale motion in the outer layer, Phys. Fluids, 11, 417–422, 1999.

Kravchenko, A. and Moin, P.: On the effect of numerical errors in large eddy simulations of turbulent flows, J. Comput. Phys., 131, 310–322, 1997.

Li, Q. and Bou-Zeid, E.: Contrasts between momentum and scalar transport over very rough surfaces, J. Fluid Mech., 880, 32–58, 2019.

Li, Q., Bou-Zeid, E., and Anderson, W.: The impact and treatment of the Gibbs phenomenon in immersed boundary method simulations of momentum and scalar transport, J. Comput. Phys., 310, 237–251, 2016a.

Li, Q., Bou-Zeid, E., and Anderson, W.: The impact and treatment of the Gibbs phenomenon in immersed boundary method simulations of momentum and scalar transport, J. Comput. Phys., 310, 237–251, 2016b.

Lilly, D.: A proposed modification of the Germano subgrid-scale closure method, Phys. Fluids, 4, 633–635, 1992.

Lozano-Durán, A. and Jiménez, J.: Effects of the computational domain on direct simulations of turbulent channels up to $Re_\tau = 4200$, Phys. Fluids, 26, 2014.

Lozano-Durán, A., Flores, O., and Jiménez, J.: The three-dimensional structure of momentum transfer in turbulent channels, J. Fluid Mech., 649, 100–130, 2012.

Lu, S. and Willmarth, W.: Measurements of the structure of the Reynolds stress in a turbulent boundary layer, J. Fluid Mech., 60, 481–511, 1973.

Majander, P. and Siikonen, T.: Evaluation of Smagorinsky-based subgrid-scale models in a finite-volume computation, Int. J. Numer. Meth. Fluids, 40, 735–774, 2002.

Margairaz, F., Giometto, M., Parlange, M., and Calaf, M.: Comparison of dealiasing schemes in large-eddy simulation of neutrally stratified atmospheric flows, Geosci. Model Dev., 11, 4069–4084, 2018.

Maronga, B., Gryschka, M., Heinze, R., Hoffmann, F., Kanani-Sühring, F., Keck, M., Ketelsen, K., Letzel, M., Sühring, M., and Raasch, S.: The parallelized large-eddy simulation model (PALM) version 4.0 for atmospheric and oceanic flows: model formulation, recent developments, and future perspectives, Geosci. Model Dev., 8, 2515–2551, 2015.

Mason, P.: Large-eddy simulation: a critical review of the technique, Q. J. R. Meteorol. Soc., 120, 1–26, 1994.

Meneveau, C., Lund, T., and Cabot, W.: A Lagrangian dynamic subgrid-scale model of turbulence, J. Fluid Mech., 319, 353–385, 1996.

Meyers, J. and B.J. Geurts, P. S.: A computational error-assessment of central finite-volume discretizations in large-eddy simulation using a Smagorinsky model, J. Comput. Phys., 227, 156–173, 2007.

Meyers, J. and Sagaut, P.: Is plane-channel flow a friendly case for the testing of large-eddy simulation subgrid-scale models?, Phys. Fluids, 19, 2007.

Meyers, J., Sagaut, P., and Geurts, B.: Optimal model parameters for multi-objective large-eddy simulations, Phys. Fluids, 18, 2006.

Mittal, R. and Moin, P.: Suitability of upwind-biased finite difference schemes for large-eddy simulation of turbulent flows, AIAA J., 35, 1997.

Moeng, C.-H.: A large-eddy simulation model for the study of planetary boundary-layer turbulence, J. Atmos. Sci., 41, 2052–2062, 1984.

Moin, P., Reynolds, W., and Ferziger, J.: Large eddy simulation of incompressible turbulent channel flow, Tech. Rep. TF-12, Thermosciences Div., Stanford University, California, 1978.

Momen, M., Bou-Zeid, E., Parlange, M., and Giometto, M.: Modulation of mean wind and turbulence in the atmospheric boundary layer by baroclinicity, Amer. Meteor. Soc., 76, 3797–3821, 2018.

Montecchia, M., Brethouwer, G., Wallin, S., Johansson, A., and Knacke, T.: Improving LES with OpenFOAM by minimising numerical dissipation and use of explicit algebraic SGS stress model, J. Turbul., 20, 697–722, 2019.

Monty, J., Stewart, J., Williams, R., and Chong, M.: Large-scale features in turbulent pipe and channel flows, J. Fluid Mech., 589, 147–156, 2007.

Monty, J., Hutchins, N., NG, H., Marusic, I., and Chong, M.: A comparison of turbulent pipe, channel and boundary layer flows, J. Fluid Mech., 632, 431–442, 2009.

Moore, G. E.: Cramming more components onto integrated circuits (Reprinted from Electronics, pg 114-117, April 19, 1965), Proceedings Of The Ieee, 86, 82–85, https://doi.org/10.1109/N-SSC.2006.4785860, papers3://publication/uuid/8E5EB7C8-681C-447D-9361-E68D1932997D, 1965.

Mukha, T., Rezaeiravesh, S., and Liefvendahl, M.: A library for wall-modelled large-eddy simulation based on OpenFOAM technology, Comput. Phys. Commun., 239, 204–224, 2019.

Nazarian, N., Martilli, A., and Kleissl, J.: Impacts of realistic urban heating, Part I: Spatial variability of mean flow, turbulent exchange and pollutant dispersion, Bound.-Layer Meteorol., 166, 367–393, 2018.

Nilsson, H., Page, M., Beaudoin, M., Gschaider, B., and Jasak, H.: The OpenFOAM turbomachinery working group, and conclusions from the turbomachinery session of the third OpenFOAM workshop, Presented at the 24^{th} symposium on hydraulic machinery and systems, IAHR, 2008.

Oke, T., Mills, G., Christen, A., and Voogt, J.: Urban climates, Cambridge University Press, 2017.

Orlandi, P.: Fluid flow phenomena: a numerical toolkit, Kluwer Academic Publishers, 2000.

Pan, Y., Chamecki, M., and Isard, S.: Large-eddy simulation of turbulence and particle dispersion inside the canopy roughness sublayer, J. Fluid Mech., 753, 499–534, 2014.

Park, G. and Moin, P.: Space-time characteristics of wall-pressure and wall shear-stress fluctuations in wall-modeled large eddy simulation, Phys. Rev. Fluids, 1, 2016.

Perot, B. and Moin, P.: Shear-free turbulent boundary layers. Part 1. Physical insights into near-wall turbulence, J. Fluid Mech., 295, 199–227, 1995.

Piomelli, U.: Wall-layer models for large-eddy simulations, Prog. Aerosp. Sci., 44, 437–446, 2008.

Piomelli, U. and Balaras, E.: Wall-layer models for large-eddy simulations, Annu. Rev. Fluid Mech., 34, 349–374, 2002.

Porté-Agel, F.: A scale-dependent dynamic model for scalar transport in large-eddy simulations of the atmospheric boundary layer, Bound.-Layer Meteorol., 112, 81–105, 2004.

Porté-Agel, F., Meneveau, C., and Parlange, M.: A scale-dependent dynamic model for large-eddy simulation: application to a neutral atmospheric boundary layer, J. Fluid Mech., 451, 261–284, 2000.

Powers, J., Klemp, J., Skamarock, W., Davis, C., Dudhia, J., Gill, D., Coen, J., and Gochis, D.: The Weather Research and Forecasting model: overview, system efforts, and future directions, Amer. Meteor. Soc., 98, 1717–1737, 2017.

Raasch, S. and Schröter, M.: PALM—A large-eddy simulation model performing on massively parallel computers, Meteorol. Z., 10, 363–372, 2001.

Raupach, M., Antonia, R., and Rajagopalan, S.: Rough-wall turbulent boundary layers, Appl. Mech. Rev., 44, 1991.

Rezaeiravesh, S. and Liefvendahl, M.: Effect of grid resolution on large eddy simulation of wall-bounded turbulence, Phys. Fluids, 30, 2018.

Rhie, C. and Chow, W.: Numerical study of the turbulent flow past an airfoil with trailing edge separation, AIAA J., 21, 1525–1532, 1983.

Salesky, S., Chamecki, M., and Bou-Zeid, E.: On the nature of the transition between roll and cellular organization in the convective boundary layer, Bound.-Layer Meteorol., 163, 41–68, 2017.

Scotti, A., Meneveau, C., and Lilly, D.: Generalized Smagorinsky model for anisotropic grids, Phys. Fluids, 5, 2306–2308, 1993.

Sharma, V., Calaf, M., and Parlange, M.: Time-adaptive wind turbine model for an LES framework, Wind Energy, 19, 939–952, 2016.

Shaw, R., Tavangar, J., and Ward, D.: Structure of the Reynolds stress in canopy layer, J. Climate Appl. Meteorol., 22, 1922–1931, 1983.

Shaw, W., Draxl, C., Mirocha, J., Muradyan, P., Ghate, V., Optis, M., and Lemke, A.: Workshop on research needs for offshore wind resource characterization, Tech. rep., U. S. Department of Energy, 2019.

Shi, L. and Yeo, D.: OpenFOAM large-eddy simulations of atmospheric boundary layer turbulence for wind engineering applications, Tech. rep., National Institute of Standards and Technology, Gaithersburg, Maryland, 2016.

Shi, L. and Yeo, D.: Large eddy simulations of model-scale turbulent atmospheric boundary layer flows, J. Eng. Mech., 143, 2017.

Sillero, J., Jiménez, J., and Moser, R.: Two-point statistics for turbulent boundary layers and channels at Reynolds numbers up to $\delta^+ \approx 2000$, Phys. Fluids, 26, 2014.

Skamarock, W., Klemp, J., Dudhia, J., Gill, D., Barker, D., Duda, M., Huang, X.-Y., Wang, W., and Powers, J.: A description of the Advanced Research WRF version 3, Tech. Rep. NCAR/TN-475+STR, National Center for Atmospheric Research, Boulder, Colorado, 2008.

Smagorinsky, J.: General circulation experiments with the primitive equations: I. The basic experiment, Mon. Weather Rev., 91, 99–164, 1963.

Stevens, R. and Meneveau, C.: Flow structure and turbulence in wind farms, Annu. Rev. Fluid Mech., 49, 311–339, 2017.

Stovall, T., Pawlas, G., and Moriarty, P.: Wind farm wake simulations in OpenFOAM, Presented at the 48^{th} AIAA Aerospace Sciences Meeting Including the New Horizons Forum and Aerospace Exposition AIAA 2010-825, American Institute of Aeronautics and Astronautics, 2010.

Stull, R.: An introduction to boundary layer meteorology, Kluwer Academic Publishers, 1988.

Sullivan, P., McWilliams, J., and Moeng, C.-H.: A subgrid-scale model for large-eddy simulation of planetary boundary-layer flows, Bound.-Layer Meteorol., 71, 1994.

Tseng, Y., Meneveau, C., and Parlange, M.: Modeling flow around bluff bodies and predicting urban dispersion using large eddy simulation, Environ. Sci. Technol., 40, 2653–2662, 2006.

Van Driest, E.: On turbulent flow near a wall, AIAA J., 23, 1007–1011, 1956.

Vuorinen, V., Keskinen, J.-P., Duwig, C., and Boersma, B.: On the implementation of low-dissipative Runge-Kutta projection methods for time dependent flows using OpenFOAM®, Comput. Fluids, 93, 153–163, 2014.

Vuorinen, V., Chaudhari, A., and Keskinen, J.-P.: Large-eddy simulation in a complex hill terrain enabled by a compact fractional step OpenFOAM® solver, Adv. Eng. Softw., 79, 70–80, 2015.

Weller, H., Tabor, G., Jasak, H., and Fureby, C.: A tensorial approach to computational continuum mechanics using object-oriented techniques, Comput. Phys., 12, 620–631, 1998.

Whiteman, C.: Mountain meteorology: fundamentals and applications, Oxford University Press, 2000.

Wu, P. and Meyers, J.: A constraint for the subgrid-scale stresses in the logarithmic region of high Reynolds number turbulent boundary layers: a solution to the log-layer mismatch problem, Phys. Fluids, 25, 2013.

Xiang, I., Park, G., and Moin, P.: Log-layer mismatch and modeling of the fluctuating wall stress in wall-modeled large-eddy simulations, Phys. Rev. Fluids, 2, 2017.

Yue, W., Meneveau, C., Parlange, M., Zhu, W., Van Hout, R., and Katz, J.: A comparative quadrant analysis of turbulence in a plant canopy, Water Resour. Res., 43, 2007a.

Yue, W., Parlange, M., Meneveau, C., Zhu, W., Hout, R., and Katz, J.: Large-eddy simulation of plant canopy flows using plant-scale representation, Bound.-Layer Meteorol., 124, 183–203, 2007b.

1 Response to reviewer 1

We thank the reviewer for his/her time and for the constructive comments, which helped improve the quality of the manuscript. We address each comment below.

1.1 Major comments

Reviewer statement 1: *The study described in the reviewed paper definitely makes sense, as it provides valuable insights regarding capabilities of a class of numerical schemes broadly used for simulations of atmospheric boundary-layer flows. It should be specifically mentioned (so far, it is not clear from the title) that techniques specifics are considered only for dynamic part of the problem (that includes Navier–Stokes and continuity equations for incompressible fluid). The study is reported in sufficient detail, and the results are analyzed quite comprehensively and candidly.*

Response: We thank the reviewer for this comment. In the Abstract it is now explicitly stated that a neutrally-stratified ABL flow without Coriolis effects is considered.

Reviewer statement 2: *The only major issue I have with the study is associated with desperation that the reader feels when—guided by the authors—she/he goes through the figures showing the results and their interpretations, and comes (together with the authors) to a conclusion that the whole situation with application of considered second-order-accurate FV schemes for LES of ABL flows in even basic setup is rather bleak (at resolutions investigated), which brings in question the entire feasibility of such schemes. The authors make some comments on what one may expect from the employed scheme with respect to its ability to reproduce particular features of the ABL turbulent flow. In my view, to make sense out of the paper findings, this discussion needs to be significantly expanded in order to provide the reader with a clear guidance regarding performance of the scheme and explain how its specific deficiencies are associated with its properties.*

Response: We thank the reviewer for this critical input. If the reviewer refers to a detailed, applied-math type analysis focusing on the impact of discretization and modeling errors on the solution, one would then need to introduce strong simplifications to make such an analysis possible (see e.g. [1] and [2]) and findings might not then be directly transferrable to the ABL flow system. The aim of this work is a different one, namely to analyze the performance of a class of general-purpose FV solvers in the *full-fledged* setup for the study of ABL flows, with a focus on their capabilities to predict physical quantities that are of interest for the ABL community without necessarily ascribing limitations thereof to specific properties of the numerical scheme. This type of

analysis is within the aim and scope of this journal, which lists "[...]full evaluations of previously published models" as one of the manuscripts' categories (see `https://www.geoscientific-model-development.net/about/manuscript_types.html`). In an efford to address the comment from the reviewer while keeping the analysis limited to the physics of the system, we identified an important limitation of the considered class of FV-solvers, which sheds light on some of the observed discrepancies and variability in flow statistics. Specifically, this class of FV solvers is not able to correctly capture the dominant momentum transport mechanism in the ABL, namely the sweep and ejection pairs, at the considered resolutions (see discussion in §3.3 as well as related comments in the Abstract and Conclusions sections of the revised manuscript, which we also report below).

> "(Abstract) At the considered resolutions, the considered class of FV-based solvers yields a poorly correlated flow field and is not able to accurately capture the dominant mechanisms responsible for momentum transport in the ABL, especially when using linear interpolation schemes for the discretization of non-linear terms. The latter consist of sweeps and ejection pairs organized side by side along the cross-stream direction, representative of a streamwise roll mode. This shortcoming leads to a misprediction of flow statistics that are relevant for ABL applications and to an enhanced sensitivity of the solution to variations in grid resolution, calling for future research aimed at reducing the impact of modeling and discretization errors."

> "(Section 3.3) As apparent from Fig. 9, the PSFD conditionally-averaged velocity field exhibits counter-rotating patterns associated with positive and negative streamwise velocity fluctuations (corresponding to the aforementioned streaks). The roll modes feature a diameters ($d \approx h$) throughout the ABL, which is consistent with findings from the literature, and positive an negative velocity fluctuations are approximately of the same magnitude ($\approx u_\tau$). From Fig. 10, it is also apparent how the considered isosurfaces extend in the streamwise direction for about $4h$. Quite surprisingly, the FV-based solver is not able to predict the roll modes, irrespective of the interpolation scheme or resolution, and the magnitude of the low-momentum streaks is also severely underpredicted across the considered cases. Further, Figs. 1 and 8 both depict a FV conditionally-averaged flow field that is poorly correlated in the cross-stream and streamwise directions, resulting in significantly smaller momentum-carrying structures. This supports previous findings from the two-point correlation maps (Fig. 4). The lack of roll modes implies that these solvers are not able to capture the fundamental mechanism supporting momentum transfer in the ABL, at least at the considered grid resolutions. This limitation can also be identified as the root cause of several of the observed problematics with the FV solutions, including the relatively high (low) streamwise-velocity skewness when using using linear (QUICK) schemes (see Fig. 2,a) and the inbalance between sweeps and ejections (Fig. 1

and Fig. 8)."

"(Conclusions) To summarize, the considered class of FV-based solvers overall predicts a flow field that is less correlated in space when compared that of the PSFD solver and is not able to capture the salient features responsible for momentum transfer in the ABL, at least at the considered grid resolutions. These limitations appear to be the root cause of many of the observed discrepancies between FV flow statistics and the reference PSFD or experimental ones, including the mispredicted streamwise-velocity skewness (Fig. 2,a), the inbalance between sweeps and ejections (Fig. 1 and Fig. 8), and the overall sensitivity of flow statistics to variations in the grid resolution."

1.2 Minor comments

Reviewer statement 1: *Page 1: It should be directly indicated in the title, or at least, in the Abstract and Introduction, that only dynamic subset of ABL governing equations is considered, so that the reader will not have hopes for seeing applications of these solvers for heat and scalar transfer equations.*

Response: Please see the response to the statement 1 in the Major comments section.

Reviewer statement 2: *Line 96: "proposed" is a wrong word here.*

Response: The sentence was edited as "Results are shown in §3 ..."

Reviewer statement 3: *Line 105: Such constancy of density is usually associated with the Boussinesq approximation, which should probably be mentioned directly.*

Response: This comment was addressed as follows: "... ρ is the (constant, under the Boussinesq approximation) fluid density, ..."

Reviewer statement 4: *Line 122: replace "observation" with "assumption".*

Response: The sentence now reads: "This conjecture is supported by the results of Majander and Siikonen (2002)."

Reviewer statement 5: *Line 138: "approximation". This is more correctly called the Boussinesq hypothesis or analogy (to distinguish from the Boussinesq approximation that refers to the density constancy).*

Response: "... (Boussinesq approximation)..." was replaced by "... (Boussinesq hypothesis)..."

Reviewer statement 6: *Line 199: replace "herein proposed" to "presented herein".*

Response: The paragraph has been rearranged and the sentence that was at line 199 does not appear anymore.

Reviewer statement 7: *Line 288: replace "statements" by "findings".*

Response: This comment was addressed and the sentence reads: "The one-dimensional spatial autocorrelation (R_{uu}), shown in Fig. 5 along the streamwise and cross-stream directions, further corroborates the above findings"

Reviewer statement 8: *Line 333: you need to specify correspondence between the u, v, w notation for velocity components and your standard u_1, u_2, u_3 notation (also in other places, where needed).*

Response: Instead of specifying a correspondence between u, v, w and u_1, u_2, u_3, the notation was unified consistently with the rest of the paper (where the subscripts x, y, z are used to denote streamwise, cross-stream, vertical directions, respectively, and correspondent vectorial components, and $(u, v, w) = (u_x, u_y, u_z)$).

Reviewer statement 9: *Figure 8: reduce font size of tick labels in x_2 direction.*

Response: The font size was reduced.

Reviewer statement 10: *Line 360: speaking of "solvers"; actually, it was a single solver that was investigated.*

Response: The "numerical framework" is indeed a single one, namely OpenFOAM®. Within this single framework, different *numerical procedures* have been considered, varying the pressure-velocity coupling method (PISO vs fractional step method), the time stepping scheme (Adam-Moulton vs Runge Kutta), and the linear interpolation scheme for the non-linear terms (linear vs QUICK). We regarded each of these procedures as "solvers", which is why we referred to "solvers". This is also standard terminology in the OpenFOAM community. Note that in the revised version of the manuscript the main analysis has now been extended to additional "solvers", and is not anymore predominantly focused on the PISO algorithm with linear interpolation scheme. We have also relaxed the terminology and we now refer to "[...]an important class of general-purpose, second order accurate FV solvers."

Reviewer statement 11: *Line 383: the verdict regarding FV-solvers; sounds too general... maybe still not all of them (a grain of optimism)?*

Response: We thank the reviewer for this comment and totally agree with it. We have tested only one specific class of FV solvers, and alternative ones such as those based on staggered grid setups or higher order discretization schemes have been shown to feature improved conservation properties and behaviors for high Reynolds number flows. We now made an effort to point out that findings proposed herein only pertain to the specific class of FV solvers that was considered (see below). We also mentioned that approaches based on a staggered grid setup might be required to improve the quality of predictions.

Abstract: "The present work assesses the quality and reliability of an important class of general-purpose, second-order accurate finite-volume (FV) solvers in the large-eddy simulation of a neutrally-stratified atmospheric boundary layer (ABL) flow."

Conclusions: "This work provides insight on the quality and reliability of an important class of general-purpose, second-order accurate FV-based solvers in wall-modeled LES of neutrally-stratified ABL flow. The FV solvers are part of the OpenFOAM® framework, make use of the divergence form of the nonlinear term, and are based on a colocated arrangement for the evaluation of the unknowns."

Conclusions: "To summarize, the considered class of FV-based solvers overall predicts a flow field that is less correlated in space when compared that of the PSFD solver and is not able to capture the salient features responsible for momentum transfer in the ABL, at least at the considered grid resolutions."

References

[1] S. Ghosal. An Analysis of Numerical Errors in Large-Eddy Simulations of Turbulence. *Journal of Computational Physics*, 125(1):187–206, apr 1996.

[2] J. Meyers, P. Sagaut, and B. J. Geurts. Optimal model parameters for multi-objective large-eddy simulations. *Physics of Fluids*, (9), 2006.

1 Response to Reviewer 2

We thank the reviewer for his/her time and for the constructive comments, which helped improve the quality of the manuscript. We address each comment below.

1.1 Major comments

Reviewer statement 1a: *This paper is about OpenFOAM rather than a generic finite-volume model. This is stated by the authors in line 195 "The results herein proposed are hence representative of the OpenFOAM solver with the standard wall-layer treatment—the set-up that is most commonly adopted when using this code". This information first comes in line 87. The relevance of the paper would be clarified and improved if this information is clearly stated earlier in the manuscript, in the abstract and maybe the title.*

Response: We thank the reviewer for this comment. We have now pointed out in the abstract, introduction and conclusions that the "class of solvers" considered herein are based on the OpenFOAM "framework" (see quotations below). We refrained from adding the *OpenFOAM* keyword in the title because findings from this study are not limited to solvers built within OpenFOAM but extend to any finite volume software/code/solver relying on these same discretization and physical-modeling procedures.

> "(Abstract) The present work assesses the quality and reliability of an important class of general-purpose, second-order accurate finite-volume (FV) solvers in the large-eddy simulation of a neutrally-stratified atmospheric boundary layer (ABL) flow. [...] Simulations are carried out within the OpenFOAM® framework, which is based on a colocated grid arrangement."

> "(Introduction) Motivated by the aforementioned needs, the present study aims at characterizing the quality and reliability of an important class of second-order accurate FV solvers for the LES of neutrally-stratified ABL flows. The analysis is conducted in the open-channel flow setup (no Coriolis acceleration) via the OpenFOAM® framework (Weller et al., 1998; De Villiers, 2006; Jasak et al., 2007)."

> "(Conclusions) [...]This work provides insight on the quality and reliability of an important class of general-purpose, second-order accurate FV-based solvers in wall-modeled LES of neutrally-stratified ABL flow. The FV solvers are part of the OpenFOAM® framework, make use of the divergence form of the nonlinear term, and are based on a colocated arrangement for the evaluation of the unknowns."

We've also add a dedicated discussion in the Methodology section on the characteristics of the OpenFOAM framework, that are shared by the considered class of solvers:

> "(Methodology) In the OpenFOAM® framework, the computational grid is colocated. Although advantageous in complex domains when compared to staggered grids (Ferziger and Peric, 2002), the colocated arrangement is known to cause difficulties with pressure-velocity coupling, hence requiring specific procedures to avoid oscillations in the solution. The standard Rhie-Chow correction (Rhie and Chow, 1983) is here adopted, which is known to negatively affeect the energy-conservation properties of central schemes (Ferziger and Peric, 2002). In addition, when approximating the integrals over the surfaces bounding each control volume (as a consequence of the Gauss divergence theorem), the unknowns are evaluated at face-centers and are assumed to be constant at each face, yielding an overall second-order spatial accuracy (Churchfield et al., 2010). Since the divergence form of the convective term is used in combination with a low-order scheme over a non-staggered grid, the solution is inherently unstable (Kravchenko and Moin, 1997). The present work makes use of the linear and the QUICK interpolation schemes (Ferziger and Peric, 2002) to evaluate the unknowns at face-centers. The numerical solver combines the PISO algorithm (Issa, 1985) for the pressure-velocity calculation and an implicit Adams–Moulton scheme for time integration (Ferziger and Peric, 2002). The performances of an alternative solver characterized by a Runge–Kutta time-advancement scheme and a projection method for the pressure-velocity coupling (Vuorinen et al., 2014) are also analyzed in the Appendix."

Reviewer statement 1b: *The abstract should also indicate that the analysis is restricted to the Smagorinsky subgrid-scale model because this is important to interpret the results.*

Response: This comment was addressed by adding the following sentence to the Abstract:

> "A series of open-channel flow simulations are performed using a static Smagorinsky model for sub-grid scale momentum fluxes and an algebraic equilibrium wall-layer model."

Reviewer statement 2: *The paper considers an "open-channel-flow set-up", and not an atmospheric boundary layer, and this information only comes in line 150. This information should also be in the abstract and the introduction.*

Response: This point was addressed by adding the following to the Abstract:

"The analysis is carried out within the OpenFOAM® framework, which is based on a colocated grid arrangement. The spatially-filtered incompressible Navier–Stokes equations are solved in an open-channel flow setup (no Coriolis acceleration)."

and the following to the Introduction:

"The analysis is conducted in the open-channel flow setup (no Coriolis acceleration) via the OpenFOAM® framework (Weller et al., 1998; De Villiers, 2006; Jasak et al., 2007)."

Reviewer statement 3: *The sensitivities that the authors study greatly depend on the resolution, measured in terms of the number of grid points (or an effective Reynolds number [Sullivan and Patton, 2011], or the ratio of the filter size to the integral length scale). Therefore, the grid size that the authors consider in the analysis should also be in the abstract, the introduction, and the conclusions. This information is important to interpret the results. The sensitivity to grid size is particularly large for the resolutions that the authors consider, which are lower than in common ABL studies. In line 165, the authors write "The chosen grid resolutions are in line with those typically used in studies of ABL flows (see, e.g., Salesky et al., 2017).", but Salesky et al. 2017 uses* 160^3 *or* 256^3*, which is a substantial difference to* 64^3 *. Resolution studies consider even larger grid sizes [Sullivan and Patton, 2011].*

Response: We agree with the point made by the reviewer. This comment was addressed by extending the analysis to cases up to 160^3 control volumes. The manuscript was edited accordingly throughout. We want to point out that while 160^3 collocation nodes in Cartesian codes run in a matter of hours for ABL flow simulations, FV-solvers supporting unstructured grid approaches are almost two orders of magnitude slower and 160^3 hence represents a state-of-the-art resolution. Overall though we agree that this resolution is relatively modest and hence results are expected to depend on this factor. This aspect of the problem has been pointed out in the Results section of the revised manuscript and in the Conclusions.

Reviewer statement 4: *The statements regarding the dependence of the results on resolution are too general. For instance, the authors write*

in line 5, "It is found that first- and second-order velocity statistics are sensitive to the grid resolution and to the details of the near-wall numerical treatment, and a general improvement is observed with horizontal grid refinement. Higher-order statistics, spectra and autocorrelations of the streamwise

velocity, on the contrary, are consistently mispredicted, regardless of the grid resolution."

in line 20, "Although mean flow and second-order statistics become acceptable provided sufficient grid resolution, the use of said solvers might prove problematic for studies requiring accurate higher-order statistics, velocity spectra and turbulence topology."

in line 70, "the excessive damping of resolved-scale energy at high wavenumber is likely to compromise their predictive capabilities for high-Reynolds ABL-flow applications."

in line 222, "Grid refinement in the horizontal directions leads to an improved match- ing between the FV and the PSFD solver, both in terms of shape and magnitude."

in line 233, "Grid refinement in the horizontal directions improves the matching between the FV-based and the PSFD-based [. . .]"

It might be more useful to say how much this dependence on resolution is, i.e., how much one particular property change when changing resolution around a particular value. In the end, as the grid is refined, we would reproduce better and better more and more properties. The important question is what grid size (or effective Reynolds number, or ratio between the filter size and the integral length scale) we need to obtain certain statistics with a given accuracy, in this case, when using OpenFOAM with a Smagorinsky subgrid-scale model in wall-bounded shear flows. For instance, for direct numerical simulations, we know that second-order methods typically need twice the resolution of spectral methods to similarly represent the variances [Moin and Mahesh, 1998]. What would be the equivalent for OpenFOAM in the model configuration considered in this study? This comment relates to what the authors write in line 83: "Note that the studies conducted with FV-based solvers are mainly focused on first- and second-order flow statistics, which are themselves not sufficient to fully characterize turbulence—and related transport—in the ABL.". What do the authors mean by "fully characterize"? For some applications, correctly representing the first- and second-order moments might be sufficient, whereas for other applications (atmospheric chemistry, wild fires) representing the spectra and LSMs might be insufficient.

Response:

We thank the reviewer for this critical input. We devoted a significant amount of efforts to this task. Both relative variations of FV profiles as a function of resolution and variations of the FV profiles with respect to reference PSFD and/or experimental ones at different resolutions were evaluated. We concluded that experimental profiles represent a good candidate for the convergence analysis at these relatively low resolutions where convergence is not strictly related to the order of accuracy of the scheme and is often non monotonic. The Results section now features several tables with quantitative measures of convergence of selected flow statistics against corresponding experimental values (streamwise velocity variances, velocity skewness, kurtosis, and integral length

scales). Note that the convergence is non-monotonic in most cases, due to the modest resolution and to the interaction of discretization and physical modeling errors, whose quantification is not trivial for this complex flow system (Meyers et al., 2006; Meyers and B.J. Geurts, 2007; Meyers and Sagaut, 2007; Ghosal, 1996). These tables nevertheless provide useful insight on the performance of FV-based solver and more quantitative information the community will benefit from. It is also apparent that higher grid resolutions are required for FV solvers to match results from the PSFD solver, or to at the least capture the dominant momentum transfer mechanisms in the channel flow system. The latter was identified as the main limitation of the considered class of FV solvers. Given that general-purpose FV solvers supporting unstructured grid setups are typically two orders of magnitude slower than PSFD solvers, going well beyond 160^3 control volumes will be a rather challenging task, and justifies the proposed study.

W ehave removed the following comment in the revised version of the manuscript: "Note that the studies conducted with FV-based solvers are mainly focused on first- and second-order flow statistics, which are themselves not sufficient to fully characterize turbulence—and related transport—in the ABL.".

Reviewer statement 5: *The introduction reads too much as a review, the focus on OpenFOAM appearing first and unexpectedly in lines 85-90. It might be useful to focus more the introduction around OpenFOAM, the half-channel configuration, and the kind of grid sizes that are considered in this analysis. This might help setting the right expectations earlier in the paper. In a similar line, the review on LSM between lines 260 to 275 might be shortened.*

Response: We thank the reviewer for this input. We have streamlined the Introduction, which now provides the motivation and objectives of the work. Details regarding the setup of the problem such as the considered grid resolutions, the half channel configuration, etc. are also briefly mentioned, but a detailed discussion of these aspects is postponed to the Methodology section (see revised manuscript).

Reviewer statement 6: *In line 187, the authors indicate that the log-layer mismatch observed in this study is a well-known problem of wall models. In line 218, the authors indicate that rms-deviations observed in this study is a well-known problem in FV-based WMLES. What is then new in this manuscript? The particularization to OpenFOAM at this particular resolution? I guess this comment relates to point 1.*

Response: We thank again the reviewer for this critical input. To the author's knowledge, this is the first assessment of the performance of this important class of FV-based solvers for the simulation of ABL flows at this level of detail/insight from a flow

physics perspective. For example, no study has previously assessed the capability of second-order accurate FV-based solvers in capturing momentum transfer mechanisms in ABL flows, how this depends on details of the numerical discretization and how it impacts relevant flow statistics. One of the key novel findings is "[...]that this class of FV-based solvers overall predicts a flow field that is less correlated in space when compared that of the PSFD solver and is not able to capture the salient features responsible for momentum transfer in the ABL, at least at the considered grid resolutions. These limitations appear to be the root cause of many of the observed discrepancies between FV flow statistics and the reference PSFD or experimental ones, including the mispredicted streamwise-velocity skewness, the inbalance between sweeps and ejections, and the overall sensitivity of flow statistics to variations in the grid resolution." With regards to the log-layer mismatch and rms-deviations: Most of the previous findings pertained to relatively low Reynolds numbers. Here we have shown that these problematics are a problem also at ABL Reynolds numbers and that procedures devised to alleviate the log-layer mismatch issue do not seem to work, which motivates further research in the field. We also showed how this mismatch depends on the numerical scheme that is used and how it depends to grid resolution, which is new. Note also that the revised manuscript has been substantially modified and now includes a detailed comparison between the performance of two interpolation schemes for the discretization of nonlinear terms, and how these schemes affect the above quantities has been commented. Further, in an efford to address this comment from the reviewer, the main contributions of this work have now been listed in the Conclusions section of the revised manuscript.

1.2 Minor comments

Reviewer statement 1: *In line 137, I am not sure I understand where* $u_\tau = \sqrt{\tau_{\alpha 2,w}|\boldsymbol{u}|/u_\alpha}$ *comes from. I do not understand equations 5 to 6. Related to it "no-slip applies at the lower surface" in line 153 is strange...*

Response: Sub-section 2.1 was expanded to provide a more detailed derivation of the wall-model. Specifically, the following lines were added:

> "Employing the no-slip condition for the velocity field, the standard FV approximation of the shear stress at the wall gives (Mukha et al., 2019)
>
> $$\tau_{i2,w} = (\nu + \nu_t)\frac{\partial u_i}{\partial x_2}\Big|_w, \quad i = 1, 3 \ ,$$
>
> where the subscript f is used to denote the evaluation at the center of the wall face, the subscript c denotes the evaluation at the center of the wall adjacent cell and Δx_2 is the distance from the wall. From the logarithmic law (Eq. 4) evaluated at the first cell-center, one can write $u_\tau = \kappa|\mathbf{u}|_c/\ln(\frac{\Delta x_2}{x_{2,0}})$. Using the definition of friction velocity $u_\tau = \sqrt{\tau_w^2}$, where τ_w is the magnitude of

the wall shear stress vector, along with Eq. 5, and rearranging, the total eddy viscosity at the wall reads..."

The sentence "... no-slip applies at the lower surface..." refers to the no-slip condition employed in combination with the wall-model.

Reviewer statement 2: *In line 154, the authors write "The kinematic viscosity is set to* 10^{-7} m^2/s *in the bulk of the flow, resulting in* $Re = 10^7$*". I think the information about Re is meaningless because the effective Reynolds number introduced by the subgrid-scale diffusivity is much smaller. As the authors later say, one can neglect the molecular viscosity against the subgrid-scale viscosity. The value of the viscosity is also a bit strange for an ABL context.*

Response: We agree with the comment. However, the simulations were run by setting the kinematic viscosity at 10^{-7} m^2/s. For this reason, the sentence was edited as follows:

> "The kinematic viscosity is set to a nominal value of 10^{-7} m^2/s, which results in an essentially inviscid flow."

Reviewer statement 3: *Adding colors in the figures might help the reader to distinguish the various cases more easily.*

Response: Colors were added to the figures.

Reviewer statement 4: *In line 227, the authors refer to the results of Del Alamo et al. 2006 regarding skewness, flatness and correlation coefficient. It might be useful to add this data to figure 3.*

Response: Del Alamo et al. 2006 do not refer to quantitative data. In Fig. 3, the measurements from Monty et al. (2009) were added.

Reviewer statement 5: *In table 3, why taking the tangent point to* $k^{-5/3}$ *to distinguish between inertial and large-scale and not some integral length scale [Pope, 2000]? Moreover,* 32 *points seem too few to distinguish an inertial subrange.*

Response: We thank the reviewer for this input. We agree that leveraging integral length scales would be a preferrable approach to distinguish between the inertial and the

production range. However, depending on the numerical setup, FV-based solvers at the considered resolutions are severely underpredicting integral length scales (see Tab. 4), thus complicating the analysis / interpretation of results. In view of this limitation, and as part of a paper-streamlining effort, we have removed this PSD analysis along with Table 3.

References

Churchfield, M., Vijayakumar, G., Brasseur, J., and Moriarty, P. (2010). Wind energy-related atmospheric boundary layer large-eddy simulation using OpenFOAM. Presented as Paper 1B.6 at the American Meteorological Society, 19$^{\text{th}}$ Symposium on Boundary Layers and Turbulence NREL/CP-500-48905, National Renewable Energy Laboratory, Colorado.

De Villiers, E. (2006). *The potential for large eddy simulation for the modeling of wall bounded flows*. PhD thesis, Imperial College of Science, Technology and Medicine.

Ferziger, J. and Peric, M. (2002). *Computational methods for fluid dynamics*. Springer.

Ghosal, S. (1996). An analysis of numerical errors in large-eddy simulations of turbulence. *J. Comput. Phys.*, 125:187–206.

Issa, R. (1985). Solution of the implicitly discretised fluid flow equations by operator-splitting. *J. Comput. Phys.*, 62:40–65.

Jasak, H., Jemcov, A., and Tukovic, Z. (2007). OpenFOAM: A c++ library for complex physics simulations. Presented at the International Workshop on Coupled Methods in Numerical Dynamics, IUC, Dubrovnik, Croatia.

Kravchenko, A. and Moin, P. (1997). On the effect of numerical errors in large eddy simulations of turbulent flows. *J. Comput. Phys.*, 131:310–322.

Meyers, J. and B.J. Geurts, P. S. (2007). A computational error-assessment of central finite-volume discretizations in large-eddy simulation using a smagorinsky model. *J. Comput. Phys.*, 227:156–173.

Meyers, J. and Sagaut, P. (2007). Is plane-channel flow a friendly case for the testing of large-eddy simulation subgrid-scale models? *Phys. Fluids*, 19.

Meyers, J., Sagaut, P., and Geurts, B. (2006). Optimal model parameters for multi-objective large-eddy simulations. *Phys. Fluids*, 18.

Rhie, C. and Chow, W. (1983). Numerical study of the turbulent flow past an airfoil with trailing edge separation. *AIAA J.*, 21:1525–1532.

Vuorinen, V., Keskinen, J.-P., Duwig, C., and Boersma, B. (2014). On the implementation of low-dissipative Runge-Kutta projection methods for time dependent flows using OpenFOAM®. *Comput. Fluids*, 93:153–163.

Weller, H., Tabor, G., Jasak, H., and Fureby, C. (1998). A tensorial approach to computational continuum mechanics using object-oriented techniques. *Comput. Phys.*, 12:620–631.